type 35 vectors for gene transfer and vaccination: efficient human cell infection and bypass of preexisting adenovirus immunity. *J Virol* 2003; **77**: 8263–8271.
15 Seshidhar Reddy P, Ganesh S, Limbach MP, Brann T, Pinkstaff A, Kaloss M *et al.* Development of adenovirus serotype 35 as a gene transfer vector. *Virology* 2003; **311**: 384–393.
16 Farina SF, Gao GP, Xiang ZQ, Rux JJ, Burnett RM, Alvira MR *et al.* Replication-defective vector based on a chimpanzee adenovirus. *J Virol* 2001; **75**: 11603–11613.
17 Reddy PS, Idamakanti N, Chen Y, Whale T, Babiuk LA, Mehtali M *et al.* Replication-defective bovine adenovirus type 3 as an expression vector. *J Virol* 1999; **73**: 9137–9144.
18 Nguyen T, Nery J, Joseph S, Rocha C, Carney G, Spindler K *et al.* Mouse adenovirus (MAV-1) expression in primary human endothelial cells and generation of a full-length infectious plasmid. *Gene Therapy* 1999; **6**: 1291–1297.
19 Hofmann C, Loser P, Cichon G, Arnold W, Both GW, Strauss M. Ovine adenovirus vectors overcome preexisting humoral immunity against human adenoviruses *in vivo*. *J Virol* 1999; **73**: 6930–6936.
20 Gaggar A, Shayakhmetov DM, Lieber A. CD46 is a cellular receptor for group B adenoviruses. *Nat Med* 2003; **9**: 1408–1412.
21 Segerman A, Atkinson JP, Marttila M, Dennerquist V, Wadell G, Arnberg N. Adenovirus type 11 uses CD46 as a cellular receptor. *J Virol* 2003; **77**: 9183–9191.
22 Sakurai F, Kawabata K, Yamaguchi T, Hayakawa T, Mizuguchi H. Optimization of adenovirus serotype 35 vectors for efficient transduction in human hematopoietic progenitors: comparison of promoter activities. *Gene Therapy* 2005; **12**: 1424–1433.
23 Peng KW, TenEyck CJ, Galanis E, Kalli KR, Hartmann LC, Russell SJ. Intraperitoneal therapy of ovarian cancer using an engineered measles virus. *Cancer Res* 2002; **62**: 4656–4662.
24 Bjorge L, Hakulinen J, Wahlstrom T, Matre R, Meri S. Complement-regulatory proteins in ovarian malignancies. *Int J Cancer* 1997; **70**: 14–25.
25 Tsujimura A, Shida K, Kitamura M, Nomura M, Takeda J, Tanaka H *et al.* Molecular cloning of a murine homologue of membrane cofactor protein (CD46): preferential expression in testicular germ cells. *Biochem J* 1998; **330** (Part 1): 163–168.
26 Johnstone RW, Loveland BE, McKenzie IF. Identification and quantification of complement regulator CD46 on normal human tissues. *Immunology* 1993; **79**: 341–347.
27 Kemper C, Leung M, Stephensen CB, Pinkert CA, Liszewski MK, Cattaneo R *et al.* Membrane cofactor protein (MCP; CD46) expression in transgenic mice. *Clin Exp Immunol* 2001; **124**: 180–189.
28 Oldstone MB, Lewicki H, Thomas D, Tishon A, Dales S, Patterson J *et al.* Measles virus infection in a transgenic model: virus-induced immunosuppression and central nervous system disease. *Cell* 1999; **98**: 629–640.
29 Lemckert AA, Sumida SM, Holterman L, Vogels R, Truitt DM, Lynch DM *et al.* Immunogenicity of heterologous prime-boost regimens involving recombinant adenovirus serotype 11 (Ad11) and Ad35 vaccine vectors in the presence of anti-ad5 immunity. *J Virol* 2005; **79**: 9694–9701.
30 Barouch DH, Pau MG, Custers JH, Koudstaal W, Kostense S, Havenga MJ *et al.* Immunogenicity of recombinant adenovirus serotype 35 vaccine in the presence of pre-existing anti-Ad5 immunity. *J Immunol* 2004; **172**: 6290–6297.
31 Okada N, Masunaga Y, Okada Y, Iiyama S, Mori N, Tsuda T *et al.* Gene transduction efficiency and maturation status in mouse bone marrow-derived dendritic cells infected with conventional or RGD fiber-mutant adenovirus vectors. *Cancer Gene Ther* 2003; **10**: 421–431.
32 Takagi T, Kitano M, Masuda S, Tokuda H, Takakura Y, Hashida M. Augmented inhibitory effect of superoxide dismutase on superoxide anion release from macrophages by direct cationization. *Biochim Biophys Acta* 1997; **1335**: 91–98.
33 Mizuguchi H, Kay MA. Efficient construction of a recombinant adenovirus vector by an improved *in vitro* ligation method. *Hum Gene Ther* 1998; **9**: 2577–2583.
34 Mizuguchi H, Kay MA. A simple method for constructing E1- and E1/E4-deleted recombinant adenoviral vectors. *Hum Gene Ther* 1999; **10**: 2013–2017.
35 Zubieta C, Schoehn G, Chroboczek J, Cusack S. The structure of the human adenovirus 2 penton. *Mol Cell* 2005; **17**: 121–135.
36 Mizuguchi H, Koizumi N, Hosono T, Ishii-Watabe A, Uchida E, Utoguchi N *et al.* CAR- or alphav integrin-binding ablated adenovirus vectors, but not fiber-modified vectors containing RGD peptide, do not change the systemic gene transfer properties in mice. *Gene Therapy* 2002; **9**: 769–776.
37 Wood M, Perrotte P, Onishi E, Harper ME, Dinney C, Pagliaro L *et al.* Biodistribution of an adenoviral vector carrying the luciferase reporter gene following intravesical or intravenous administration to a mouse. *Cancer Gene Ther* 1999; **6**: 367–372.
38 Huard J, Lochmuller H, Acsadi G, Jani A, Massie B, Karpati G. The route of administration is a major determinant of the transduction efficiency of rat tissues by adenoviral recombinants. *Gene Therapy* 1995; **2**: 107–115.
39 Cattaneo R. Four viruses, two bacteria, and one receptor: membrane cofactor protein (CD46) as pathogens' magnet. *J Virol* 2004; **78**: 4385–4388.
40 Mrkic B, Pavlovic J, Rulicke T, Volpe P, Buchholz CJ, Hourcade D *et al.* Measles virus spread and pathogenesis in genetically modified mice. *J Virol* 1998; **72**: 7420–7427.
41 Johansson L, Rytkonen A, Bergman P, Albiger B, Kallstrom H, Hokfelt T *et al.* CD46 in meningococcal disease. *Science* 2003; **301**: 373–375.
42 Maisner A, Zimmer G, Liszewski MK, Lublin DM, Atkinson JP, Herrler G. Membrane cofactor protein (CD46) is a basolateral protein that is not endocytosed. Importance of the tetrapeptide FTSL at the carboxyl terminus. *J Biol Chem* 1997; **272**: 20793–20799.
43 Ichida S, Yuzawa Y, Okada H, Yoshioka K, Matsuo S. Localization of the complement regulatory proteins in the normal human kidney. *Kidney Int* 1994; **46**: 89–96.
44 Sinn PL, Williams G, Vongpunsawad S, Cattaneo R, McCray Jr PB. Measles virus preferentially transduces the basolateral surface of well-differentiated human airway epithelia. *J Virol* 2002; **76**: 2403–2409.
45 Segerman A, Arnberg N, Erikson A, Lindman K, Wadell G. There are two different species B adenovirus receptors: sBAR, common to species B1 and B2 adenoviruses, and sB2AR, exclusively used by species B2 adenoviruses. *J Virol* 2003; **77**: 1157–1162.
46 Seya T, Hara T, Iwata K, Kuriyama S, Hasegawa T, Nagase Y *et al.* Purification and functional properties of soluble forms of membrane cofactor protein (CD46) of complement: identification of forms increased in cancer patients' sera. *Int Immunol* 1995; **7**: 727–736.
47 Smith TA, Idamakanti N, Rollence ML, Marshall-Neff J, Kim J, Mulgrew K *et al.* Adenovirus serotype 5 fiber shaft influences *in vivo* gene transfer in mice. *Hum Gene Ther* 2003; **14**: 777–787.
48 Koizumi N, Mizuguchi H, Sakurai F, Yamaguchi T, Watanabe Y, Hayakawa T. Reduction of natural adenovirus tropism to mouse liver by fiber-shaft exchange in combination with both CAR- and alphav integrin-binding ablation. *J Virol* 2003; **77**: 13062–13072.
49 Anderson BD, Nakamura T, Russell SJ, Peng KW. High CD46 receptor density determines preferential killing of tumor cells by oncolytic measles virus. *Cancer Res* 2004; **64**: 4919–4926.
50 Kimura Y, Yanagimachi R. Intracytoplasmic sperm injection in the mouse. *Biol Reprod* 1995; **52**: 709–720.

51 Perry AC, Wakayama T, Kishikawa H, Kasai T, Okabe M, Toyoda Y *et al.* Mammalian transgenesis by intracytoplasmic sperm injection. *Science* 1999; **284**: 1180–1183.
52 Hosono T, Mizuguchi H, Katayama K, Xu ZL, Sakurai F, Ishii-Watabe A *et al.* Adenovirus vector-mediated doxycycline-inducible RNA interference. *Hum Gene Ther* 2004; **15**: 813–819.
53 Xu ZL, Mizuguchi H, Ishii-Watabe A, Uchida E, Mayumi T, Hayakawa T. Optimization of transcriptional regulatory elements for constructing plasmid vectors. *Gene* 2001; **272**: 149–156.
54 Sakai M, Nishikawa M, Thanaketpaisarn O, Yamashita F, Hashida M. Hepatocyte-targeted gene transfer by combination of vascularly delivered plasmid DNA and *in vivo* electroporation. *Gene Therapy* 2005; **12**: 607–616.
55 Sakurai F, Nishioka T, Saito H, Baba T, Okuda A, Matsumoto O *et al.* Interaction between DNA–cationic liposome complexes and erythrocytes is an important factor in systemic gene transfer via the intravenous route in mice: the role of the neutral helper lipid. *Gene Therapy* 2001; **8**: 677–686.

ARTICLE

doi:10.1016/j.ymthe.2005.10.007

Quantitative Comparison of Intracellular Trafficking and Nuclear Transcription between Adenoviral and Lipoplex Systems

Susumu Hama,[1,2] Hidetaka Akita,[1,2] Rie Ito,[1] Hiroyuki Mizuguchi,[3] Takao Hayakawa,[4] and Hideyoshi Harashima[1,2,*]

[1]*Graduate School of Pharmaceutical Sciences, Hokkaido University, Sapporo, Hokkaido 060-0812, Japan*
[2]*CREST, Japan Science and Technology Corporation, Tokyo, Japan*
[3]*Laboratory of Gene Transfer and Regulation, National Institute of Biomedical Innovation, Osaka 567-0085, Japan*
[4]*Pharmaceuticals and Medical Devices Agency, Tokyo 100-0013, Japan*

**To whom correspondence and reprint requests should be addressed. Fax: +81 11 706 4879. E-mail: harasima@pharm.hokudai.ac.jp.*

Available online 20 December 2005

To develop nonviral gene vectors that are sufficient for clinical application, it is necessary to understand why and to what extent nonviral vectors are inferior to viral vectors, which in general show a more efficient transfection activity. This study describes a systematic and quantitative comparison of the cellular uptake and subsequent intracellular distribution (e.g., endosome/lysosome, cytosol, and nucleus) of exogenous DNA transfected by viral and nonviral vectors in living cells, using a combination of TaqMan PCR and a recently developed confocal image-assisted three-dimensionally integrated quantification method. As a model, adenovirus (Ad) and Lipofectamine Plus (LFN) were used for comparison since they are highly potent and widely used viral and nonviral vectors, respectively. The findings indicate that the efficiency of cellular uptake for LFN is significantly higher than that for Ad. Once taken up by a cell, Ad exhibited comparable endosomal escape and slightly higher nuclear transfer efficiency compared with LFN. In contrast, LFN requires 3 orders of magnitude more intranuclear gene copies to exhibit a transgene expression comparable to that of the Ad, suggesting that the difference in transfection efficiency principally arises from differences in nuclear transcription efficiency and not from a difference in intracellular trafficking between Ad and LFN.

Key Words: adenovirus, nonviral vector, lipoplex, quantification, intracellular trafficking, gene vector

INTRODUCTION

Numerous nonviral vectors have been developed for use in gene therapy for intractable diseases [1,2]. However, low transfection efficiency still remains a bottleneck, preventing its use in clinical applications. It is generally considered that transfection activity is rate limited to a great extent, by a variety of intracellular processes such as endosomal escape, nuclear transfer, and intranuclear transcription.

Along with evolution of life during the past hundreds of millions of years, DNA and RNA viruses have also evolved and have developed sophisticated mechanisms for controlling intracellular trafficking for the efficient delivery of their genomes to nuclei in host cells for symbiosis. Although some nonviral vectors have been evolutionally developed since the first proposal of the concept of gene therapy over 30 years ago [3], this history is overwhelmingly short. Therefore, the transfection efficiency of a virus vector is, in general, more prominent than that of a nonviral vector [4]. To improve nonviral vectors, quantitative information concerning why and to what extent the nonviral vector is inferior to the viral one is essential.

For the quantification of intracellular trafficking, we and other researchers have developed methodology to quantify the amount of plasmid DNA in the nucleus by nuclear fractionation followed by the polymerase chain reaction (PCR) [5–7]. This quantification revealed an important lesson showing that it is necessary to optimize not only the nuclear delivery of plasmid DNA, but also intranuclear transcription efficiency, since transgene expression is remarkably saturated against nucleus-delivered pDNA. In contrast to the nucleus, very few reports are available concerning the amount of pDNA in the

1525-0016/$30.00

endosome/lysosome compartment, and therefore, it is very difficult to evaluate the efficiency of endosomal release. Although the subcellular fractionation of endosomes/lysosomes may solve this issue, many problems, such as the complicated protocol, uncertainties associated with the recovery of the endosomal fraction, and mutual contamination may prevent this strategy from becoming a practical application.

We recently developed a novel strategy, the confocal image-assisted three-dimensionally integrated quantification (CIDIQ) method, which enables the distribution of exogenous DNA in endosome/lysosome, cytosol, and nucleus to be quantified simultaneously in individual cells with sequential *Z*-series images captured by confocal laser scanning microscopy [8,9]. Since intracellular trafficking investigated by CIDIQ can readily explain the differences in transgene expression by various nonviral vectors, this method is useful for identifying the rate-limiting barriers to gene expression.

In the present study, we applied it to the systematic and quantitative comparison of the intracellular distribution of exogenous genes transfected by viral vector and nonviral vector in living cells. It enabled us to examine the rate-limiting processes associated with nonviral vectors that limit their transfection efficiency. As model vectors, we used adenovirus (Ad) and Lipofectamine Plus (LFN), highly potent and widely used viral and nonviral vectors (lipoplex), respectively, in the comparative study.

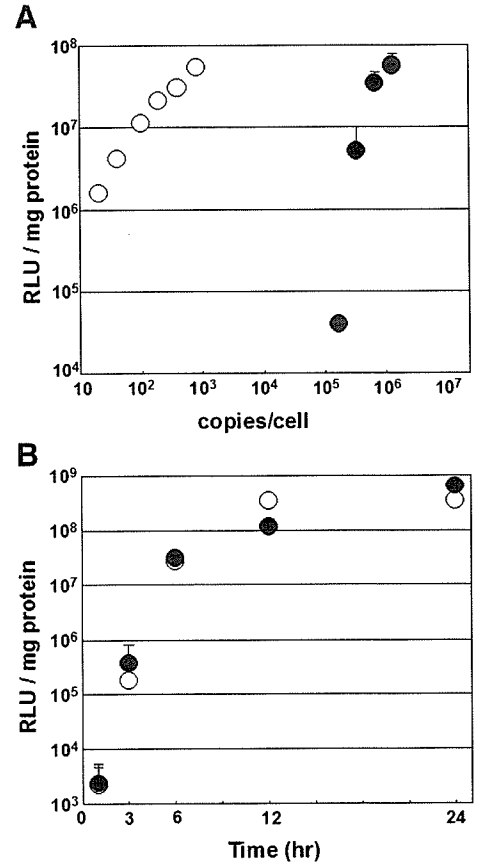

FIG. 1. Dose–response curve and time course of luciferase gene expression in A549 cells transfected by Ad and LFN. (A) Luciferase gene expression in cells transfected by Ad (○) or LFN (●) was measured 6 h after incubation at the indicated dose. (B) Transfection activities were measured at indicated times after incubation with a dose of 200 (○) or 6.7×10^5 copies/cell (5 pg/cell) (●). The vertical axis represents luciferase activity expressed as relative light units (RLU)/mg protein. These data represent the mean values and standard deviation of three experiments.

RESULTS

Comparison of Transfection Activity between Ad and LFN

We initially compared the time-dependent and applied dose-dependent transfection activity between Ad and LFN. The methodology used to determine the applied dose in terms of luciferase gene copies is described under Materials and Methods. As shown in Fig. 1A, transgene expression is increased in a dose-dependent manner for both vectors 6 h after incubation. In subsequent experiments, we fixed the dose of plasmid DNA (pDNA) in the LFN-mediated transfection at 6.7×10^5 copies/cell (5 pg/cell) based on the manufacturer's recommended protocol, from which approximately 5×10^7 RLU/mg protein of luciferase activity was exhibited. In the case of Ad, we fixed the dose at 200 copies/cell, since comparable levels of transgene expression can be achieved at this dose. As shown in Fig. 1B, both vectors exhibited quite comparable time courses for transgene expression at these doses, suggesting that LFN is a potent system for the delivery of pDNA to the nucleus with a speed comparable to that of Ad. However, it should be emphasized that LFN requires 3 orders of magnitude more gene copies than the Ad to achieve comparable gene expression (Fig. 1A). Furthermore, the difference in the required dose for achieving a comparable level of transgene expression is dependent on the expression level. In a comparison of the expression of 1×10^6 RLU/mg protein, approximately 10,000-fold more copies of plasmid DNA were required for LFN, and at a lower transgene expression level, the difference was even greater. This is due to the nonlinear relationship between the dose and the transfection efficiency in LFN and is also sometimes observed in various nonviral vectors [10].

Quantification of an Intracellular Distribution of pDNA and Ad DNA

We then quantified the intracellular distribution of pDNA or Ad by a combination of TaqMan PCR and CIDIQ [8]. The procedures used to determine the distribution of exogenous DNA transfected by LFN and Ad are

doi:10.1016/j.ymthe.2005.10.007

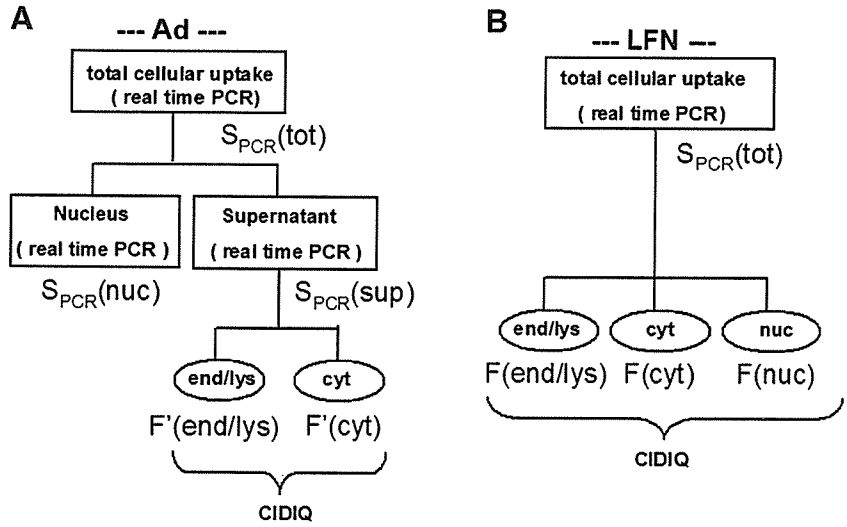

FIG. 2. Schematic diagram illustrating the concept for the quantification of intracellular distribution of exogenous genes. Subcellular distributions of exogenous DNA transfected by Ad and LFN were quantified by TaqMan PCR and CIDIQ analysis as illustrated in (A) and (B), respectively. (A) Total cellular uptake (S_{PCR}(tot) and nuclear-delivered Ad DNA (S_{PCR}(nuc)) were quantified by TaqMan PCR. Distributions of Ad in endosome/lysosome and cytosol (F'(end/lys) and F'(cyt), respectively) were also determined by CIDIQ. The copy numbers in the endosome/lysosome and cytosol fractions were calculated as S_{PCR}(sup) multiplied by F'(end/lys) and F'(cyt), respectively. (B) S_{PCR}(tot) was first determined by TaqMan PCR in terms of gene copies. The fraction of plasmid DNA in the endosome/lysosome, cytosol, and nucleus was determined by CIDIQ.

illustrated in Figs. 2A and 2B. We determined the total cellular uptake (S_{PCR}(tot)) first by TaqMan PCR in terms of gene copies. In the case of LFN, we determined the fraction of plasmid DNA in the endosome/lysosome, cytosol, and nucleus by CIDIQ (Fig. 2B). A schematic diagram illustrating the principal of CIDIQ analysis is shown in Fig. 4A. After the transfection of rhodamine-labeled pDNA, we stained the endosome/lysosome and nucleus with LysoSensor DND-189 and Hoechst 33342, respectively, to discriminate the subcellular localization of the pDNA (typical images are exhibited in Fig. 4C). We transferred each 8-bit TIFF image to Image-Pro Plus version 4.0 (Media Cybernetics, Inc., Silver Spring, MD, USA) to quantify the total brightness and pixel area of each region of interest. Since we have previously shown that the majority of rhodamine-labeled pDNA was present in the form of clusters in the cytosol and nucleus at 1 h (a typical image is shown in Fig. 4C), we used the pixel area of each cluster in endosomes/lysosomes, s_i(end/lys); cytosol, s_i(cyt); and nucleus, s_i(nuc) as an index of the amount of pDNA [8]. The detailed methodology for the calculation of the fraction of pDNA in the endosome/lysosome, cytosol, and nucleus (F(end/lys), F(cyt), and F(nuc), respectively) is described under Materials and Methods. The copy number in each organelle is calculated as S_{PCR}(tot) multiplied by the fraction in each organelle (Fig. 2B).

We also determined intracellular distribution for the Ad by CIDIQ (a typical image is shown in Fig. 4B), in which the pixel areas of the Texas red-labeled Ad are used as an index of the amount of Ad. However, the nuclear pixels cannot serve as an index for the amount of Ad DNA, since it is dissociated from the fluorescence-labeled capsid proteins when it is internalized via the nuclear pore complex [11]. Therefore, we determined nucleus-associated Ad DNA (S_{PCR}(nuc)) beforehand by nuclear isolation, followed by TaqMan PCR (Fig. 2A). In this case, the supernatant from the nuclear isolation procedure (S_{PCR}(sup)) includes DNA in both the endosomal/lysosome and the cytosol fractions. The copy numbers in these fractions are calculated as S_{PCR}(sup) multiplied by the fractions calculated by CIDIQ (F'(end/lys) and F'(cyt), respectively).

Comparison of the Cellular Uptake Process between LFN and Ad

We first quantified the cellular uptake of pDNA transfected with LFN and Ad in terms of copy numbers of luciferase genes by TaqMan PCR. Since the nuclear delivery of exogenous DNA is achieved within 1 h for both of vectors [8,12–14], we evaluated cellular uptake and the following intracellular distribution at 1 h to compare the initial disposition of DNA. As a result, the number of copies of pDNA taken up by the cell for LFN was approximately 15,000-fold more than that for Ad (Fig. 3). After we normalized the cellular uptake by the applied dose, more

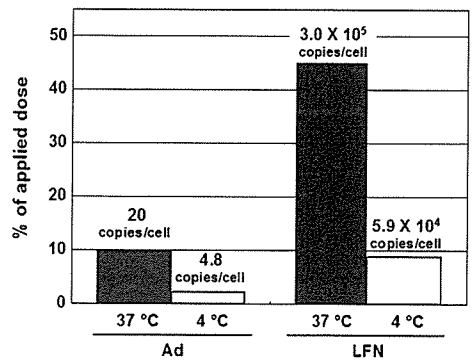

FIG. 3. Quantification of cellular uptake and cellular binding of Ad and LFN in A549 cells. A549 cells were incubated with adenovirus or LFN at 37 and 4 °C for 1 h to evaluate cellular uptake and cellular binding, respectively. Associated genes were quantified in terms of copy number of luciferase genes by TaqMan PCR. Cellular association was normalized by number of cells, which was quantified by the number of copies of the genomic β-actin gene.

than 40% of the pDNA was taken up by the cell, whereas for the Ad DNA, this value was only 10% (Fig. 3).

Total cellular uptake is a hybrid parameter of cell surface binding and the internalization rate constant (k_{int}). Therefore, we measured the cellular binding of pDNA and Ad by incubation at 4°C for 1 h. In the case of LFN, 8.8% of the applied pDNA was attached to the cell surface, whereas the corresponding value was only 2.4% for the Ad (Fig. 3). When the k_{int}, denoted as the total cellular uptake (Fig. 3) divided by the cell surface binding (Fig. 3), were compared, LFN was found to exhibit a value comparable to that of Ad (5.1 and 4.2 h^{-1}, respectively).

Comparison of Intracellular Trafficking between Ad and LFN

Concerning the intracellular distribution after transfection with LFN, 47.4% of the pDNA was in the endosome/lysosome fraction and a large part of the pDNA had already escaped from this compartment (Figs. 4E and 5) within 1 h. In addition, we observed significant nuclear distribution (13.5%) (Figs. 4E and 5). This is consistent with rapid gene expression within 3 h (Fig. 1B). Multiplying these fractions by the S_{PCR}(tot), we calculated the copy numbers in each organelle as shown in Fig. 5.

In the Ad, we determined nuclear fraction by nuclear isolation, followed by TaqMan PCR. After incubation at 37°C at 1 h, 54.2% of the Ad genome was experimentally recovered from the nuclear fraction. To avoid a situation in which the nuclear delivery of the Ad genome was overestimated, we estimated the efficiency of contamination of Ad in the nucleus during the nuclear isolation with cells that were incubated with Ad at 4°C, at which temperature nuclear delivery was largely excluded. After incubation at 4°C for 1 h, we fractionated the nucleus and quantified cell surface-bound and nucleus-associated Ad. As a result, we calculated the percentage of nuclear Ad to cell surface-bound Ad to be 17.6%. Thus, 17.6% of the nuclear fraction, corresponding to contamination during the isolation process, was subtracted from the experimentally determined nuclear fraction after the incubation at 37°C (54.2%). As a result, we calculated that 36.6% of the total cellular uptake (7.3 copies/nucleus) of DNA reached the nucleus (Fig. 5). Other portions (12.7 copies/cell; 63.4% of the total cellular uptake) were recovered from the supernatant fractions (S_{PCR}(sup)), which include the endosome/lysosome and cytosol fractions. A CIDIQ analysis showed that the fractions in the endosome/lysosome (F'(end/lys)) and the cytosol (F'(cyt)) compared to the supernatant were 47.9 and 52.1%, respectively. Taking these data into consideration, we calculated the numbers of Ad gene copies in the endosome/lysosome and cytosol as 6.1 copies/cell (30.3% of the total cellular uptake) and 6.6 copies/cell (33.1% of the total cellular uptake), respectively (Figs. 4D and 5). The efficiency of the endosomal escape and nuclear translocation calculated from the data shown in the circle graph in Fig. 5 is summarized in Table 1. We calculated the efficiency of endosomal escape as the fraction that escaped from the endosome/lysosome (nuclear fraction plus cytoplasmic fraction) divided by the total cellular uptake. Similarly, we determined the efficiency of nuclear translocation as the nuclear fraction divided by the fraction that escaped from the endosome/lysosome (nuclear fraction plus cytoplasmic fraction). As a result, the efficiency of endosomal escape is only slightly higher for Ad. In contrast, the efficiency of nuclear translocation is considerably higher for Ad.

Finally, comparing the nuclear delivery of DNA, 5600-fold more gene copies are delivered to the nucleus in the case of LFN. We calculated transcription efficiency as the expression divided by the gene copies in the nucleus as shown in Fig. 5. It was shown that Ad is 8100 times more efficient than LFN in nuclear transcription.

This conclusion is also applicable to HeLa cells (Table 2). To exhibit a comparable transgene expression, LFN also requires 3 orders of magnitude more gene copies (200 vs 1.4×10^6 copies/cell). Under these conditions, approximately 4100 times more gene copies reach the nucleus, and therefore, the transcription efficiency of Ad was approximately 7000 times higher than that of LFN.

Discussion

In the present study, intracellular trafficking and the intranuclear transcription of exogenous DNA transfected by viral and nonviral vectors were quantitatively evaluated. Ad and LFN were used as model vectors in the comparison, since they are both highly potent and widely used vectors. As a result, we found that LFN can accomplish transgene expression comparable to that of the Ad vector, when the protocol is optimized. However, the dose of pDNA in terms of luciferase gene copies under these conditions was 3 orders of magnitude more than that of Ad. Therefore, it would be worthwhile to clarify which of the intracellular processes is rate limiting for LFN.

First, the cellular uptake process was compared. Calculated from the applied dose and cellular uptake (Fig. 3), LFN exhibited significantly higher cellular uptake efficiency than Ad (approximately 45% vs 10%). Further comparison of the cellular binding efficiency by incubation at 4°C (Fig. 3) indicated that the efficient cellular uptake in the case of LFN can be attributed to efficient cellular binding, but not to the internalization rate constant (k_{int}). The superior cellular surface binding in the case of LFN can be explained by differences in the binding mechanism. Binding of the Ad is based on specific ligand–receptor interactions between the fiber protein and the coxsackievirus and Ad receptor and between the RGD motif in the penton base and the integrin receptors [15]. Therefore, the maximum binding is dependent on the total number of these receptors. In

doi:10.1016/j.ymthe.2005.10.007

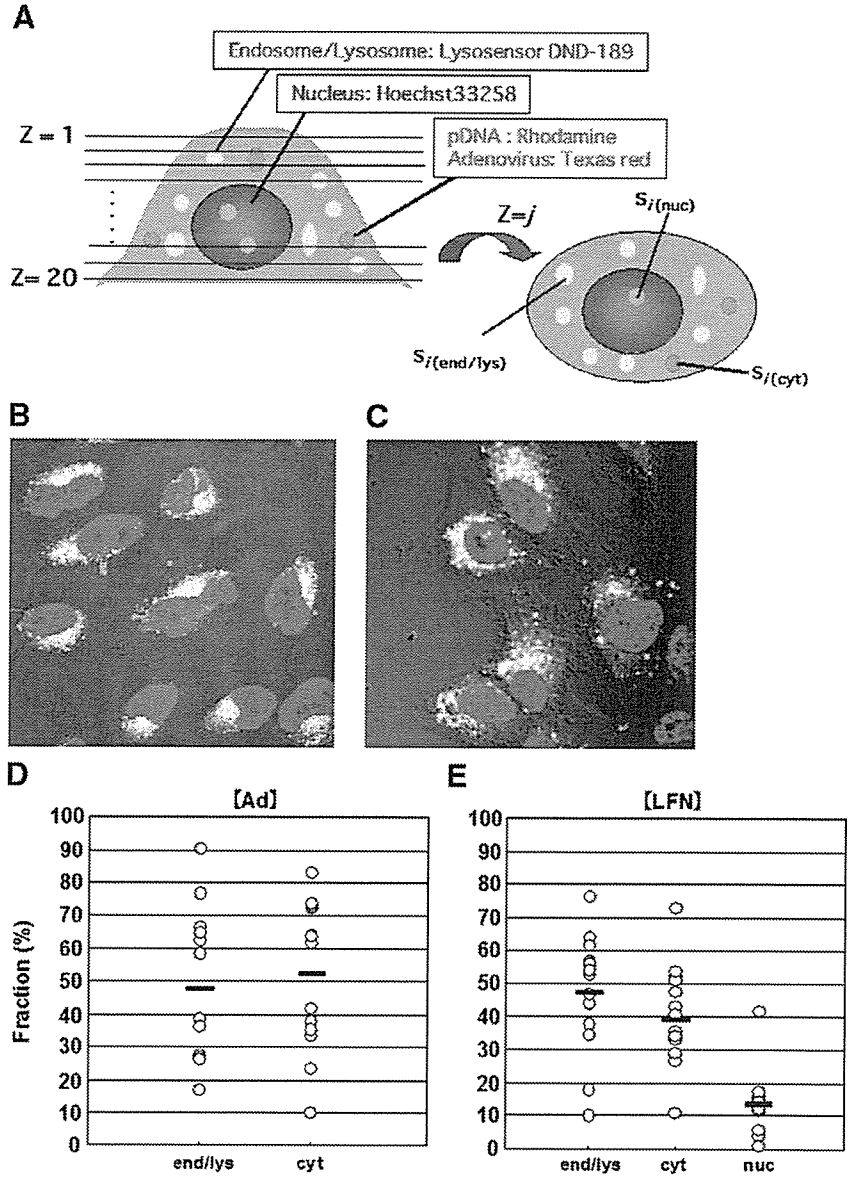

FIG. 4. Quantification of the intracellular distribution of exogenous genes by CIDIQ analysis. (A) Schematic diagram of the CIDIQ analysis is illustrated. 20 Z-series images were captured by confocal laser scanning microscopy. The pixel areas corresponding to the pDNA in each x–y plane ($Z = j$), $s_j(k)$, were summed for the respective compartments and are denoted as $S'_{Z=j}(k)$, where k represents each compartment (e.g., endosome/lysosome, cytosol, and nucleus). $S'_{Z=j}(k)$ in each x–y-plane image was further integrated to obtain $S(k)$, which represents the total pixel area localized in each compartment (k) in one cell. All of the $S(k)$ values were combined to calculate the S(tot), reflecting the total pixel area in a cell. $F(k)$, representing the fraction of plasmid DNA in each compartment to the whole cell, was calculated as $S(k)$ divided by S(tot). (B and C) Typical images for the confocal laser scanning microscopy used in the CIDIQ analysis in Ad and LFN are shown. Texas red-labeled Ad or rhodamine-labeled pDNA (red) were transfected into A549 cells. Endosome/lysosome and nucleus compartments were stained with LysoSensor DND-189 (green) and Hoechst 33342 (blue), respectively. (D and E) Fractions of DNA in the endosome/lysosome, cytosol, and nucleus determined by the strategy illustrated in Fig. 2 after transfection with Ad and LFN are shown. These values represent the mean values of 15 individual cells.

contrast, the pDNA/LFN complex can bind to the entire cell surface area via electrostatic interactions. Concerning the k_{int} value, it has recently been reported that Ad enters, not only via clathrin-mediated endocytosis [16,17], but also via macropinocytosis [18,19], which is actively driven by signal transduction after the binding of the RGD motif to the integrin receptor for cellular entry [20–22]. Therefore, the internalization of Ad appears to be a highly efficient process. The k_{int} value of LFN was comparable to that of Ad. A recent study indicated that a certain type of nonviral vector was taken up by cells, not only by the classical endocytosis pathway [23,24], but also by another pathway such as macropinocytosis [25]. Presumably, multiple pathways are also responsible to the cellular uptake of LFN, and this results in an internalization rate constant comparable to that of Ad. Concerning intracellular trafficking, various types of cellular uptake processes must be considered. Since only acidic compartments were stained by LysoSensor DND-189, the involvement of nonacidic vesicular compartments such as caveola was excluded from the analysis. To analyze the contribution of acidic vesicular transport (i.e., clathrin-mediated endocytosis and macropinocytosis [26]) to total vesicular transport, plasma membranes were nonspecifically labeled with PKH-26 (Sigma). After incubation for 1 h, all of the labels on the plasma membrane were internalized and detected as clustered forms. Dual staining with PKH-26 and LysoSensor DND-189 revealed that approximately 70% of the PKH-26 clusters were colocalized with LysoSensor DND-189, suggesting that a major

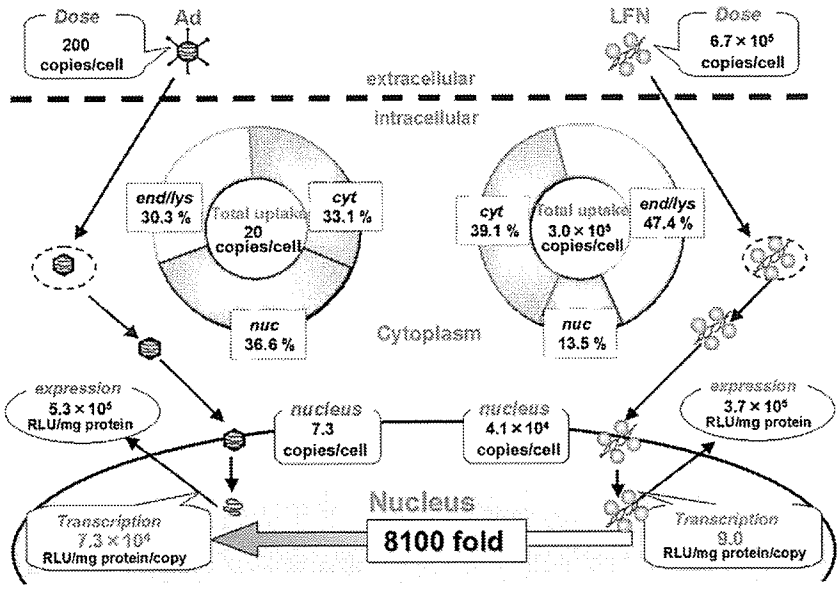

FIG. 5. Summary of the quantitative comparison of intracellular trafficking in A549 cells between Ad and LFN. These values were quantified by TaqMan PCR and CIDIQ analysis.

part (~70%) of the vesicular transport system was acidic compartments (data not shown). In addition, it appears that the size of the lipoplex (generally more than 200 nm [27,28]) is too large to be taken up via nonacidic vesicular transport such as caveolin-mediated endocytosis (~60 nm) and clathrin- and caveolin-independent endocytosis (~90 nm) [29]. Therefore, we conclude that the staining of vesicular compartments by LysoSensor DND-189 is useful for tracing the main intracellular trafficking of vectors, although it is possible that pDNA taken up via a nonacidic compartment may unexpectedly participate in the efficient trafficking pathway. The mechanism for the efficient internalization rate of the LFN remains to be clarified.

Concerning endosomal escape, it was considered that the dismantling of Ad particles in response to the low endosomal pH is closely related to this event [16,30]. Wiethoff *et al.* have recently shown that partial disassembly of the Ad capsid triggers the release of protein VI, which then lyses the endosomal membrane structure [31]. LFN also had an efficiency comparable to that of adenovirus (Table 1). LFN consists of polycationic lipid 2,3-dioleyloxy-*N*-[2(spermincarboxamido)ethyl]-*N*,*N*-dimethyl-1-propanaminium trifluoroacetate (DOSPA) and corn-shape lipid dioleoyl phosphatidylethanolamine (DOPE). A highly efficient endosomal escape of LFN, as high as that of Ad, was then synergistically achieved by the proton sponge effect [32] derived from secondary amines in DOSPA, along with the fusogenic effect [33,34] of DOPE, whereas their strategies were different.

In contrast, once it escapes into the cytosol, adenovirus delivers its DNA to the nucleus more efficiently than LFN. Although LFN can rapidly deliver its DNA to the nucleus presumably due to the electric interaction of cationic lipid and negatively charged lipids of the nuclear membrane [35], it is likely that the cytoplasmic delivery of Ad is more sophisticated. It has previously been shown that Ad utilizes a microtubule network to pass through the cytoplasm into the nucleus [36,37]. Furthermore, Ad binds to the nuclear pore complex receptor CAN/Nup214 and, thereafter, inserts the genomic DNA into the nucleus with the assistance of

TABLE 1: Comparison of the efficiencies of endosomal escape and nuclear translocation between Ad and LFN

	Ad	LFN
Endosomal escape; (cytosol + nucleus)/total	0.70	0.53
Nuclear translocation; nucleus/(nucleus + cytosol)	0.53	0.26

The efficiencies of endosomal escape and nuclear translocation were calculated from the results in Fig. 5 (circle graph) as the fraction that escaped from the endosome/lysosome (nuclear fraction plus cytoplasmic fraction) divided by total cellular uptake and as the nuclear fraction divided by the fraction that escaped from the endosome/lysosome, respectively.

TABLE 2: Comparison of nuclear delivery and transcription efficiency between Ad and LFN in HeLa cells

	Ad	LFN
Dose (copies/cell)	200	1.4×10^6
Nuclear DNA (copies/cell)	4.1	1.7×10^4
Transgene expression (RLU/mg protein)	2.3×10^7	1.3×10^7
Transcription efficiency (RUL/mg protein/copy)	5.7×10^6	810

The numbers of gene copies required to exhibit comparable transgene expression were quantified by TaqMan PCR and are represented as copies/cell. Nuclear DNA in Ad- and LFN-mediated transfection was determined following the procedure illustrated in Fig. 2. Transcription efficiency was calculated as the expression divided by the gene copies in the nucleus.

doi:10.1016/j.ymthe.2005.10.007

nuclear histone H1 cells and the importin family proteins of the host cells [11,38]. Such types of multiple/active delivery systems in adenovirus may be responsible for its efficient nuclear delivery.

Finally, the intranuclear transcription of DNA, when transfected with Ad, is 8100 times higher than that of LFN. Considering that the CMV promoter, luciferase (GL3), and BGH polyadenylation sequences in pDNA and the Ad genome are identical to one another, two explanations are possible. One is that the nuclear DNA introduced by the LFN is so well condensed that the transcription process is inhibited. It is generally accepted that the release of pDNA from the vectors is the rate-determining process for transgene expression [39]. In fact, transgene expression after the nuclear microinjection of DNA as a lipoplex was reported to be severely limited [28,40]. The other possibility is that the Ad genome structure and/or proteins coded in the Ad genome affect transgene expression. Since almost all of the E1/E3 region was deleted from the Ad genome, other factors such as the inverted terminal repeat sequence [41], terminal protein [42], and various proteins derived from the E4 region [43,44] may be involved in the improvement in transcription and nuclear stability. Currently, it has been reported that terminal proteins interact with the nuclear matrix, where they play an important role in nuclear transcription [42]. To evaluate the potential of pDNA vis-a-vis adenovirus DNA in the transcription process, adenoviral DNA was purified by treatment with guanidine, followed by sucrose gradient centrifugation [45]. The nuclear microinjection of 10 copies of plasmid DNA and Ad genome encoding the green fluorescent protein revealed that the Ad genome exhibited only a slightly higher transgene expression compared with plasmid DNA (approximately 35% vs 25%), suggesting that these two types of DNA are equivalent in the transcription process (S. Hama *et al.*, unpublished observation). As a result, the difference in decondensation in the nucleus is a more plausible hypothesis for explaining the difference in intranuclear transcription.

The remarkable difference in transcription activity was also found in HeLa cells, indicating that this phenomenon is generally applicable to various cells. Very recently, it was also shown that the intranuclear transcription of plasmid DNA introduced by nonviral vectors such as polyethylenimine was much lower than that of viral vectors. This conclusion is then generally applicable to various types of current nonviral vectors [46].

Collectively, we were able successfully to quantify the intracellular trafficking and intranuclear transcription of viral and nonviral vectors. LFN delivers pDNA to the nucleus with a comparable speed and exhibits transgene expression comparable to that of the Ad vector. However, LFN requires 3 orders of magnitude more pDNA than the Ad to exert similar transfection activities. Surprisingly, this remarkable difference principally arises from differences in nuclear transcription efficiency. This is the first systematic and quantitative comparison of the intracellular distribution of the exogenous genes introduced by a viral vector and a nonviral vector. Such quantitative comparisons will be useful for developing new generations of nonviral vectors.

MATERIALS AND METHODS

General. To prepare the reporter gene vector for the pDNA (pcDNA3.1-GL3), an insert fragment encoding luciferase (GL3) was obtained by *Hin*dIII/*Xba*I digestion of the pGL3-Basic vector (Promega, Madison, WI, USA) and ligated to the *Hin*dIII/*Xba*I-digested site of pcDNA3.1 (Invitrogen, Carlsbad, CA, USA). LFN was from Invitrogen Corp. Other chemicals used were commercially available and reagent grade products. As to the viral vector, the $E1^-$, $E3^-$, replication-deficient serotype 5 adenovirus, in which an expression cassette is inserted in the E_1 position, was used [47]. The expression cassette consists of a cytomegalovirus promoter/enhancer, cDNA encoding luciferase (GL3), and BGH polyadenylation sequences, which are also encoded in the pDNA used in the LFN-mediated transfection.

Quantification of luciferase gene copies by TaqMan PCR. To determine the applied particle titer of the Ad in terms of copy number of luciferase gene, Ad was dismantled by vortexing with 0.1% SDS/10 mM Tris–HCl/5 mM EDTA treatment. The number of luciferase gene copies was determined by TaqMan PCR with a 100-fold diluted sample solution. As a reference, a dilution series of pDNA3.1-GL3 was run along with the virus sample. It was confirmed that 0.001% SDS and 0.05 mM EDTA had no effect on the luciferase gene amplification by TaqMan PCR. The luciferase gene region of Ad genomic DNA or pDNA was amplified and quantified by TaqMan PCR (ABI Prism 7700 sequence detection system; Applied Biosystems). The sequence of the probe was 5′-CCGCTGAATTG-GAATCCATCTTGCTC-3′ with FAM as a fluorescent dye on the 5′ end and TAMRA as a fluorescence quencher dye labeled on the 3′ end. This probe is designed to anneal to the target between the sense primer (5′-TTGACCGCCTGAAGTCTCTGA-3′) and the antisense primer (5′-ACACCTGCGTCGAAGATGTTG-3′) in the luciferase sequence of the Ad genome and pDNA.

For the quantification of cellular uptake and nuclear delivery of the luciferase genes, DNA was purified from cell lysates or an isolated nucleus by means of a GenElute Mammalian Genome DNA Miniprep kit (Sigma–Aldrich, St. Louis, MO, USA) and subjected to the TaqMan PCR with ABI Prism 7700 sequence detection system. The isolation of nuclei followed a previous report [6,7]. Briefly, cells were suspended in 0.5 ml of lysis buffer (0.5% Nonidet P-40, 10 mM NaCl, 3 mM $MgCl_2$, 10 mM Tris–HCl buffer; pH 7.4) to dissolve the plasma membrane, and the nuclear fraction was then isolated by centrifugation at 1400*g* for 5 min. This treatment (washing) was repeated twice, and the final pellet was used as the nuclear fraction. The high recovery of the Ad genome (>90%) by DNA purification with the GenElute Mammalian Genome DNA Miniprep kit was confirmed by comparison with the luciferase gene amplification by TaqMan PCR.

The number of β-actin DNAs was also determined by the ABI Prism 7700 sequence detection system. PCR was performed according to the manufacturer's instructions with 0.5 μM each forward, 5′-TGCGTGACAT-TAAGGAGAAGCTGTG-3′, and reverse, 5′-CAGCGGAACCGCTCATTGC-CAATGG-3′, primers and the QuantiTect SYBR Green PCR Master Mix (Qiagen, Hilden, Germany). A linear relationship between the number of cells and the threshold cycle for the β-actin gene amplification was confirmed (data not shown).

CIDIQ analysis. In the case of LFN-mediated transfection, the pDNA fraction in the endosome/lysosome, cytosol, and nucleus compared to the total cellular association was assessed by CIDIQ, as described in a recent report [8]. After the transfection of rhodamine-labeled pDNA, the endo-

some/lysosome and nucleus were stained with LysoSensor DND-189 and Hoechst 33342, respectively, to discriminate the subcellular localization of pDNA. Each 8-bit TIFF image was transferred to Image-Pro Plus version 4.0 (Media Cybernetics, Inc.) to quantify the total brightness and pixel area of each region of interest. For data analysis, the pixel areas of each cluster in endosomes/lysosomes, s_i(end/lys); cytosol, s_i(cyt); and nucleus, s_i(nuc) were separately summed for each x–y plane and are denoted as $S'_{Z=j}$(end/lys), $S'_{Z=j}$(cyt), and $S'_{Z=j}$(nuc), respectively. The values of $S'_{Z=j}$(end/lys), $S'_{Z=j}$(cyt), and $S'_{Z=j}$(nuc) in each x–y plane were further summed and are denoted as S(end/lys), S(cyt), and S(nuc), respectively. These parameters represent the total amount of pDNA in each compartment in an individual cell. Furthermore, the total area of the pDNA, denoted as S(tot), was calculated by integrating the S(end/lys), S(cyt), and S(nuc). This value represents the total cellular uptake of pDNA. The fractions of pDNA present in endosomes/lysosomes, cytosol, and nucleus compared to the whole cell are denoted as F(end/lys), F(cyt), and F(nuc), which were calculated as S(end/lys), S(cyt), and S(nuc) divided by S(tot), respectively.

For quantification of the intracellular distribution of Ad, Texas red-labeled Ad was used in the CIDIQ analysis. The nuclear delivery of Ad DNA (S_{PCR}(nuc)) was quantified beforehand by nuclear fractionation, followed by the TaqMan PCR [6]. The supernatant fraction S_{PCR}(sup) contains Ad DNA in the endosome/lysosome and cytosol. Therefore, the fractions in these organelles were quantified by CIDIQ. In this case, S(sup), which represents the Ad DNA in the supernatant fraction in the nucleus isolation experiment, was calculated by integrating the S'(end/lys) and S'(cyt). The fractions of Ad DNA present in endosomes/lysosomes and cytosol compared to the supernatant are denoted as F'(end/lys) and F'(cyt), which were calculated as S'(end/lys) and S'(cyt) divided by S(sup), respectively. Numbers of gene copies in these organelles were determined by multiplying each fraction by S_{PCR}(sup).

ACKNOWLEDGMENTS

This work was supported in part by Grants-in-Aid for Scientific Research (B) and Grant-in-Aid for Young Scientists (B) from the Ministry of Education, Culture, Sports, Science, and Technology of Japan and by Grants-in-Aid for Scientific Research on Priority Areas from the Japan Society for the Promotion of Science.

RECEIVED FOR PUBLICATION JUNE 11, 2005; REVISED SEPTEMBER 30 2005; ACCEPTED OCTOBER 1, 2005.

REFERENCES

1. Lai, C. M., Lai, Y. K., and Rakoczy, P. E. (2002). Adenovirus and adeno-associated virus vectors. *DNA Cell Biol.* **21:** 895–913.
2. Yoshida, J., *et al.* (2004). Human gene therapy for malignant gliomas (glioblastoma multiforme and anaplastic astrocytoma) by in vivo transduction with human interferon beta gene using cationic liposomes. *Hum. Gene Ther.* **15:** 77–86.
3. Friedmann, T., and Roblin, R. (1972). Gene therapy for human genetic disease? *Science* **175:** 949–955.
4. Dinser, R., *et al.* (2001). Comparison of long-term transgene expression after non-viral and adenoviral gene transfer into primary articular chondrocytes. *Histochem. Cell Biol.* **116:** 69–77.
5. Oh, Y. K., *et al.* (2002). Polyethylenimine-mediated cellular uptake, nucleus trafficking and expression of cytokine plasmid DNA. *Gene Ther.* **9:** 1627–1632.
6. Tachibana, R., *et al.* (2002). Quantitative analysis of correlation between number of nuclear plasmids and gene expression activity after transfection with cationic liposomes. *Pharm. Res.* **19:** 377–381.
7. Tachibana, R., Harashima, H., Shinohara, Y., and Kiwada, H. (2001). Quantitative studies on the nuclear transport of plasmid DNA and gene expression employing nonviral vectors. *Adv. Drug Delivery Rev.* **52:** 219–226.
8. Akita, H., Ito, R., Khalil, I. A., Futaki, S., and Harashima, H. (2004). Quantitative three-dimensional analysis of the intracellular trafficking of plasmid DNA transfected by a nonviral gene delivery system using confocal laser scanning microscopy. *Mol. Ther.* **9:** 443–451.
9. Masuda, T., Akita, H., and Harashima, H. (2005). Evaluation of nuclear transfer and transcription of plasmid DNA condensed with protamine by microinjection: the use of a nuclear transfer score. *FEBS Lett.* **579:** 2143–2148.
10. Moriguchi, R., *et al.* (in press). Non-linear pharmacodynamics in a non-viral gene delivery system: positive non-linear relationship between dose and transfection efficiency. *J. Controlled Release*.
11. Trotman, L. C., Mosberger, N., Fornerod, M., Stidwill, R. P., and Greber, U. F. (2001). Import of adenovirus DNA involves the nuclear pore complex receptor CAN/Nup214 and histone H1. *Nat. Cell Biol.* **3:** 1092–1100.
12. Leopold, P. L., *et al.* (1998). Fluorescent virions: dynamic tracking of the pathway of adenoviral gene transfer vectors in living cells. *Hum. Gene Ther.* **9:** 367–378.
13. Miyazawa, N., *et al.* (1999). Fiber swap between adenovirus subgroups B and C alters intracellular trafficking of adenovirus gene transfer vectors. *J. Virol.* **73:** 6056–6065.
14. Nakano, M. Y., and Greber, U. F. (2000). Quantitative microscopy of fluorescent adenovirus entry. *J. Struct. Biol.* **129:** 57–68.
15. Meier, O., and Greber, U. F. (2003). Adenovirus endocytosis. *J. Gene Med* **5:** 451–462.
16. Greber, U. F., Willetts, M., Webster, P., and Helenius, A. (1993). Stepwise dismantling of adenovirus 2 during entry into cells. *Cell* **75:** 477–486.
17. Varga, M. J., Weibull, C., and Everitt, E. (1991). Infectious entry pathway of adenovirus type 2. *J. Virol.* **65:** 6061–6070.
18. Imelli, N., Meier, O., Boucke, K., Hemmi, S., and Greber, U. F. (2004). Cholesterol is required for endocytosis and endosomal escape of adenovirus type 2. *J. Virol.* **78:** 3089–3098.
19. Meier, O., *et al.* (2002). Adenovirus triggers macropinocytosis and endosomal leakage together with its clathrin-mediated uptake. *J. Cell Biol.* **158:** 1119–1131.
20. Amyere, M., *et al.* (2000). Constitutive macropinocytosis in oncogene-transformed fibroblasts depends on sequential permanent activation of phosphoinositide 3-kinase and phospholipase C. *Mol. Biol. Cell.* **11:** 3453–3467.
21. Araki, N., Johnson, M. T., and Swanson, J. A. (1996). A role for phosphoinositide 3-kinase in the completion of macropinocytosis and phagocytosis by macrophages. *J. Cell Biol.* **135:** 1249–1260.
22. Li, E., Stupack, D., Klemke, R., Cheresh, D. A., and Nemerow, G. R. (1998). Adenovirus endocytosis via alpha(v) integrins requires phosphoinositide-3-OH kinase. *J. Virol.* **72:** 2055–2061.
23. Zhou, X., and Huang, L. (1994). DNA transfection mediated by cationic liposomes containing lipopolylysine: characterization and mechanism of action. *Biochim. Biophys. Acta* **1189:** 195–203.
24. Zuhorn, I. S., Kalicharan, R., and Hoekstra, D. (2002). Lipoplex-mediated transfection of mammalian cells occurs through the cholesterol-dependent clathrin-mediated pathway of endocytosis. *J. Biol. Chem.* **277:** 18021–18028.
25. Goncalves, C., *et al.* (2004). Macropinocytosis of polyplexes and recycling of plasmid via the clathrin-dependent pathway impair the transfection efficiency of human hepatocarcinoma cells. *Mol. Ther.* **10:** 373–385.
26. Wadia, J. S., Stan, R. V., and Dowdy, S. F. (2004). Transducible TAT-HA fusogenic peptide enhances escape of TAT-fusion proteins after lipid raft macropinocytosis. *Nat. Med.* **10:** 310–315.
27. Joshee, N., Bastola, D. R., and Cheng, P. W. (2002). Transferrin-facilitated lipofection gene delivery strategy: characterization of the transfection complexes and intracellular trafficking. *Hum. Gene Ther.* **13:** 1991–2004.
28. Zabner, J., Fasbender, A. J., Moninger, T., Poellinger, K. A., and Welsh, M. J. (1995). Cellular and molecular barriers to gene transfer by a cationic lipid. *J. Biol. Chem.* **270:** 18997–19007.
29. Conner, S. D., and Schmid, S. L. (2003). Regulated portals of entry into the cell. *Nature* **422:** 37–44.
30. Medina-Kauwe, L. K. (2003). Endocytosis of adenovirus and adenovirus capsid proteins. *Adv. Drug Delivery Rev.* **55:** 1485–1496.
31. Wiethoff, C. M., Wodrich, H., Gerace, L., and Nemerow, G. R. (2005). Adenovirus protein VI mediates membrane disruption following capsid disassembly. *J. Virol.* **79:** 1992–2000.
32. Boussif, O., *et al.* (1995). A versatile vector for gene and oligonucleotide transfer into cells in culture and in vivo: polyethylenimine. *Proc. Natl. Acad. Sci. USA* **92:** 7297–7301.
33. Bailey, A. L., and Cullis, P. R. (1997). Membrane fusion with cationic liposomes: effects of target membrane lipid composition. *Biochemistry* **36:** 1628–1634.
34. Wattiaux, R., Jadot, M., Warnier-Pirotte, M. T., and Wattiaux-De Coninck, S. (1997). Cationic lipids destabilize lysosomal membrane in vitro. *FEBS Lett.* **417:** 199–202.
35. Daum, G. (1985). Lipids of mitochondria. *Biochim. Biophys. Acta* **822:** 1–42.
36. Suomalainen, M., Nakano, M. Y., Boucke, K., Keller, S., and Greber, U. F. (2001). Adenovirus-activated PKA and p38/MAPK pathways boost microtubule-mediated nuclear targeting of virus. *EMBO J.* **20:** 1310–1319.
37. Suomalainen, M., *et al.* (1999). Microtubule-dependent plus- and minus end-directed motilities are competing processes for nuclear targeting of adenovirus. *J. Cell Biol.* **144:** 657–672.
38. Greber, U. F., *et al.* (1997). The role of the nuclear pore complex in adenovirus DNA entry. *EMBO J.* **16:** 5998–6007.
39. Bieber, T., Meissner, W., Kostin, S., Niemann, A., and Elsasser, H. P. (2002). Intracellular route and transcriptional competence of polyethylenimine–DNA complexes. *J. Controlled Release* **82:** 441–454.
40. Pollard, H., *et al.* (1998). Polyethylenimine but not cationic lipids promotes transgene delivery to the nucleus in mammalian cells. *J. Biol. Chem.* **273:** 7507–7511.
41. Hatfield, L., and Hearing, P. (1991). Redundant enhancements in the adenovirus type 5

doi:10.1016/j.ymthe.2005.10.007

inverted terminal repeat promote bidirectional transcription *in vitro* and are important for virus growth *in vivo*. *Virology* **184:** 265–276.
42. Fredman, J. N., and Engler, J. A. (1993). Adenovirus precursor to terminal protein interacts with the nuclear matrix in vivo and in vitro. *J. Virol.* **67:** 3384–3395.
43. Endter, C., and Dobner, T. (2004). Cell transformation by human adenoviruses. *Curr. Top. Microbiol. Immunol.* **273:** 163–214.
44. Tauber, B., and Dobner, T. (2001). Adenovirus early E4 genes in viral oncogenesis. *Oncogene* **20:** 7847–7854.
45. Sharp, P. A., Moore, C., and Haverty, J. L. (1976). The infectivity of adenovirus 5 DNA–protein complex. *Virology* **75:** 442–456.
46. Varga, C. M., *et al.* (2005). Quantitative comparison of polyethylenimine formulations and adenoviral vectors in terms of intracellular gene delivery processes. *Gene Ther.* **12:** 1023–1032.
47. Mizuguchi, H., *et al.* (2001). A simplified system for constructing recombinant adenoviral vectors containing heterologous peptides in the HI loop of their fiber knob. *Gene Ther.* **8:** 730–735.

Cancer Gene Therapy (2006) 13, 393–405

www.nature.com/cgt

ORIGINAL ARTICLE

Tumor suppressive efficacy through augmentation of tumor-infiltrating immune cells by intratumoral injection of chemokine-expressing adenoviral vector

N Okada[1], A Sasaki[1], M Niwa[1], Y Okada[2], Y Hatanaka[3], Y Tani[3], H Mizuguchi[4], S Nakagawa[5], T Fujita[1] and A Yamamoto[1]

[1]*Department of Biopharmaceutics, Kyoto Pharmaceutical University, Misasagi, Yamashina-ku, Kyoto, Japan;* [2]*Research Institute for Microbial Diseases, Osaka University, Suita, Osaka, Japan;* [3]*Department of Biomedical Science, DakoCytomation Company Ltd, Nishinotouin-higashiiru, Shijo-dori, Shimogyo-ku, Kyoto, Japan;* [4]*National Institute of Biomedical Innovation, Ibaraki, Osaka, Japan;* [5]*Department of Biopharmaceutics, Graduate School of Pharmaceutical Sciences, Osaka University, Suita, Osaka, Japan*

Our goal in the present study was to evaluate antitumor effects and frequency of tumor-infiltrating immune cells upon intratumoral injection of RGD fiber-mutant adenoviral vector (AdRGD) encoding the chemokines CCL17, CCL19, CCL20, CCL21, CCL22, CCL27, XCL1, and CX3CL1. Among eight kinds of chemokine-expressing AdRGDs, AdRGD-CCL19 injection most efficiently induced infiltration of T cells into established B16BL6 tumor parenchyma, whereas most of these T cells were perforin-negative in immunohistochemical analysis. Additionally, the growth of AdRGD-CCL19-injected tumors decreased only slightly as well as that of other tumors treated with each chemokine-expressing AdRGD, which indicated that accumulation of naive T cells in tumor tissue does not effectively damage the tumor cells. Tumor-bearing mice, in which B16BL6-specific T cells were elicited by dendritic cell-based immunization, demonstrated that intratumoral injection of AdRGD-CCL17, -CCL22, or -CCL27 could considerably suppress tumor growth and attract activated T cells. On the other hand, AdRGD-CCL19-injection in the immunized mice showed slight increase of tumor-infiltrating T cells compared to treatment using control vector. Collectively, although AdRGD-mediated chemokine gene transduction into established tumors would be very useful for augmentation of tumor-infiltrating immune cells, a combinational treatment that can systemically induce tumor-specific effector T cells is necessary for satisfactory antitumor efficacy.
Cancer Gene Therapy (2006) **13,** 393–405. doi:10.1038/sj.cgt.7700903; published online 14 October 2005

Keywords: chemokine; adenoviral vector; tumor-infiltrating immune cell; melanoma

Introduction

Tumor cells that generally accumulate mutations in the genome express molecules different qualitatively and quantitatively from normal cells. An immunosurveillance system for these molecules, known as the tumor-associated antigen (TAA), plays an important role in the elimination of cancer cells during the initial stage.[1–3] However, because tumor cells are inherently autologous cells and their immunogenicity is very weak as compared with pathogens (non-self) invading from the outside world, malignant tumor cells can evade immunosurveillance and then infringe upon various biological functions by uncontrollable proliferation and metastasis. In addition, several soluble factors secreted from tumor cells are known to induce failure in the host's immune function.[4,5] Therefore, amelioration of illness exhibiting a growing tumor mass is difficult by innate immunity alone. Development of immunotherapy for cancer would involve the establishment of a methodology capable of enhancing recognition of tumor cell characteristics (differences from normal cells) by a patient's immune system, and accumulating activated immune effector cells at a local tumor site.

Cancer immunotherapy research has steadily progressed towards clinical application through cooperative fundamental research and clinical studies that have focused on adoptive transfer of lymphokine-activated killer cells or tumor-specific cytotoxic T lymphocytes (CTLs)[6,7] and administration of TAA-component vaccine,[8] TAA-coding DNA vaccine,[9] genetically modified tumor cell-based vaccine,[10,11] or TAA-delivered dendritic cell (DC)-based vaccine.[12–14] Although these approaches can induce and amplify tumor immunity in patients, satisfactory efficacy, including marked tumor regression or complete response, has not been previously reported in a clinical setting. One potential cause of these disappointing results

Correspondence: Dr N Okada, Department of Biopharmaceutics, Kyoto Pharmaceutical University, 5 Nakauchi-cho, Misasagi, Yamashina-ku, Kyoto 607-8414, Japan.
E-mail: okada@mb.kyoto-phu.ac.jp
Received 27 April 2005; revised 11 July 2005; accepted 17 July 2005; published online 14 October 2005

is insufficient investigation and understanding of methods that improve accumulation of immune effector cells in tumor tissue. The principal objective of most conventional studies of cancer immunotherapy has been efficient induction and activation of effector cells. Therefore, even if effector cells that exhibited the ability to kill tumor cells were adequately induced in a patient, the efficacy of cancer immunotherapy would be considerably limited if effector cells were unable to infiltrate tumor tissue and come in contact with tumor cells. Innovative approaches capable of better controlling biodistribution of immune effector cells are needed to overcome the limitations of current therapy.

Chemokine–chemokine receptor coupling controls leukocytic migration and infiltration of local sites through cooperation with various cell adhesion molecules.[15] Chemokines, which are small (8–14 kDa) secreted basic proteins, comprise a superfamily that contains four subgroups: C chemokine, CC chemokine, CXC chemokine, and CX3C chemokine.[16] These subgroups are defined by the position of conservative cysteine residues in the N-terminal and interactions with their specific receptors, which belong to the superfamily of seven-transmembrane domain G-protein-coupled receptors.[17,18] Initially, chemokines were identified as a group of cytokines capable of enhancing migration of neutrophils and monocytes, and functional analysis has focused on their role in inflammation. In the late 1990s, the sequence of immune chemokine, which primarily affects lymphocytes and DCs, was identified by a bioinformatics technique that used an EST database search. To date, more than 50 chemokines have been identified. Chemokines are now considered important molecules for cancer immunotherapy, which is based on the eradication of tumor cells as a consequence of interaction with immune cells that have migrated and accumulated in tumor tissues.[19–24]

We previously demonstrated that tumor cells transduced with RGD fiber-mutant adenoviral vector (AdRGD) encoding a chemokine gene could adequately secrete a biologically active chemokine, and that *in vitro* transfection established several chemokines as promising candidates for cancer treatment in three murine tumor models.[25,26] Although the inoculation of chemokine-transduced tumor cells was very useful for screening antitumor effects through the promotion of chemokine secretion in tumor tissue, direct *in vivo* injection of chemokine-expressing vector into tumor tissue is required for the development of effective chemokine-based cancer immunogenetherapy. Thus, in the present study, we attempted to investigate tumor suppressive effects of intratumoral injection of AdRGD encoding murine chemokines CCL17, CCL19, CCL20, CCL21, CCL22, CCL27, XCL1, and CX3CL1, and identify immune cells capable of infiltrating tumor tissue in the murine B16BL6 melanoma model.

Materials and methods

Cell lines and mice

HEK293 cells, the helper cell line for AdRGD propagation, were purchased from ATCC (Manassas, VA) and cultured in Dulbecco's modified Eagle's medium supplemented with 10% fetal bovine serum (FBS) and antibiotics. Murine melanoma B16BL6 cells (H-2^b) were obtained from JCRB cell bank (Tokyo, Japan) and grown in minimum essential medium supplemented with 7.5% FBS and antibiotics. EL4 cells, a T-lymphoma cell line of C57BL/6 origin, and YAC-1 cells, a lymphoma cell line highly sensitive to natural killer (NK) cells, were purchased from ATCC and maintained in RPMI 1640 medium supplemented with 10% FBS, 50 μM 2-mercaptoethanol, and antibiotics. Female C57BL/6 mice (H-2^b), age 7–8 weeks, were purchased from Japan SLC Inc. (Hamamatsu, Japan), and were held under specific pathogen-free conditions. Animal experimental procedures were in accordance with the Osaka University guidelines for the welfare of animals in experimental neoplasia.

Vectors

Replication-deficient AdRGD was based on the adenovirus serotype 5 backbone with deletions of E1 and E3 regions. The RGD sequence for αv-integrin-targeting was inserted into the HI loop of the fiber knob using a two-step method as previously described.[27] Eight murine chemokine-expressing AdRGDs (AdRGD-CCL17, -CCL19, -CCL20, -CCL21, -CCL22, -CCL27, -XCL1, and -CX3CL1),[25,26] gp100-expressing AdRGD (AdRGD-gp100),[28] and luciferase-expressing AdRGD (AdRGD-Luc)[27] were previously constructed by an improved *in vitro* ligation method.[27,29,30] All recombinant AdRGDs were propagated in HEK293 cells, purified by two rounds of cesium chloride gradient ultracentrifugation, dialyzed, and stored at −80°C. Titers of infective AdRGD particles (plaque-forming unit; PFU) were evaluated by the end point dilution method using HEK293 cells.

Generation and viral transduction of DCs

DCs were prepared according to the method of Lutz *et al*.[31] with slight modification. Briefly, bone marrow cells flushed from the femurs and tibias of C57BL/6 mice were seeded at $0.5–1 \times 10^7$ cells per sterile 100-mm bacterial grade culture dish in 10 ml of RPMI 1640 containing 10% FBS, 40 ng/ml recombinant murine granulocyte/macrophage colony-stimulating factor (kindly provided by KIRIN Brewery Co., Ltd, Tokyo, Japan), 50 μM 2-mercaptoethanol, and antibiotics. On day 3, another 10 ml of culture medium was added to the dish for medium replenishment. On day 6, 10 ml of the culture supernatant was collected and centrifuged at 1500 r.p.m. for 5 min at room temperature, and the pellet was resuspended in 10 ml of fresh culture medium, and then returned to the original dish to conserve unattached cells. On day 8, nonadherent cells were harvested and used as DCs. In transduction using AdRGD-gp100, DCs were suspended at a concentration of 5×10^6 cells/ml in FBS-free RPMI 1640 and placed in a 50-ml conical tube. AdRGD-gp100 was added at 25 PFU/cell, the suspension was mixed well, and the tube was incubated at 37°C for 2 h with occasional gentle agitation. The cells were washed three times and resuspended with phosphate-buffered

saline (PBS), and used in subsequent experiments as gp100/DCs.

Protocol for intratumoral injection of chemokine-expressing AdRGD (Protocol-1)
C57BL/6 mice were intradermally inoculated with 4×10^5 B16BL6 cells in the right flank. After 6 days, established tumors with diameters of 5–7 mm were injected with each vector at 3×10^8 PFU in 50-μl PBS.

Protocol for intratumoral injection of chemokine-expressing AdRGD in combination with gp100/DC immunization (Protocol-2)
B16BL6 cells were intradermally inoculated into C57BL/6 mice in the right flank at 4×10^5 cells/mouse. The next day, the mice were intradermally injected with 10^6 gp100/DCs in the left flank. Then, the 5–7 mm in diameter tumors were injected with each vector at 3×10^8 PFU in 50-μl PBS.

Evaluation of tumor growth
The major and minor axes of the tumors treated with Protocol-1 or -2 were measured using microcalipers, and tumor volume was calculated by the following formula: (tumor volume; mm^3) = (major axis; mm) × (minor axis; $mm)^2 \times 0.5236$. The mice were euthanized when one of the two measurements was greater than 20 mm.

Histopathological and immunohistochemical examination of tumor sections
Tumor-bearing mice were killed 2 days after the intratumoral injection of chemokine-expressing AdRGD in Protocol-1 or -2. For histopathological examination, the tumor nodules were harvested, placed in neutral 10% formalin/PBS, and embedded in paraffin. Sections (5 μm in thickness) were prepared for hematoxylin and eosin (HE) staining. For immunohistochemical analysis, the fresh tumor nodules were embedded in OCT compound (Sakura Finetechnical Co., Ltd, Tokyo, Japan), and frozen in liquid nitrogen. Frozen sections (5 μm in thickness) were fixed in 4% paraformaldehyde, washed with PBS, and then stored at −80°C until following immunostaining procedures. Only in the sections for Ki-67 detection, antigen retrieval treatment was performed with target retrieval solution pH6 (DakoCytomation Co., Ltd, Kyoto, Japan) at 95°C for 10 min. The immunostaining procedures, which included blocking for endogenous peroxidase activity with peroxidase blocking solution (DakoCytomation), blocking for nonspecific binding of the subsequently used immunoreagents with 5% bovine serum albumin, incubation with optimal dilution of antibody, incubation of reagent(s) for detection, and development with 3,3′-diaminobenzidine, were carried out on automated immunostaining system (Autostainer Plus, DakoCytomation). Between all incubation steps, the tumor sections were washed with Tris-bufferd saline containing Tween-20. The following antibodies were used as primary antibody; rat anti-mouse Ki-67 monoclonal antibody (mAb) (TEC-3; DakoCytomation), rat anti-mouse CD34 mAb (RAM34; BD Biosciences, San Jose, CA), rat anti-mouse F4/80 mAb (C1:A3-1; Serotec Co., Ltd, Sapporo, Japan), rabbit anti-human CD3 polyclonal antibody (DakoCytomation), rabbit anti-asialoGM1 polyclonal antibody (Wako Pure Chemical Industries, Ltd, Osaka, Japan), rat anti-mouse CD4 mAb (RM4-5; BD Biosciences), rat anti-mouse CD8 mAb (KT15; Serotec Co., Ltd), rat anti-mouse perforin mAb (P1-8; DakoCytomation), or hamster anti-mouse CD11c mAb (N418; CHEMICON International, Inc., Temecula, CA). Rat anti-mouse Ki-67 mAb was detected with biotinylated anti-rat Ig (DakoCytomation) and horseradish peroxidase (HRP)-conjugated streptavidin (DakoCytomation). Rabbit anti-human CD3 polyclonal antibody and rabbit anti-asialoGM1 polyclonal antibody were detected with ENVISION+ Rabbit/HRP (DakoCytomation). Hamster anti-mouse CD11c mAb was detected with HRP-conjugated anti-hamster Ig (BD Biosciences) and CSA II System (DakoCytomation). Other primary antibodies were detected with HRP-conjugated anti-rat Ig (Santa Cruz Biotechnology, Inc., Santa Cruz, CA) and CSA II System. The sections were finally counterstained with hematoxylin. The number of immunostained cells in six fields per specimen was counted under a light microscope using × 400 magnification.

Europium-release assay for cytolytic activity of CTLs
B16BL6 cells were intradermally inoculated into C57BL6 mice in the right flank at 4×10^5 cells/mouse. The next day, the mice were intradermally injected with 10^6 gp100/DCs or PBS in the left flank. At 1 week after immunization, nonadherent splenocytes were prepared from these tumor-bearing mice and restimulated *in vitro* using B16BL6 cells, which were cultured in media containing 100 U/ml recombinant murine interferon (IFN)-γ (PeproTech EC Ltd, London, UK) for 24 h and inactivated with 50 μg/ml mitomycin C at 37°C for 30 min, at an effector:stimulator ratio of 10:1 in RPMI 1640 supplemented with 10% FBS, 50 μM 2-mercaptoethanol, and antibiotics. After 5 days, the splenocytes were collected and used as effector cells. Target cells (IFN-γ-stimulated B16BL6, IFN-γ-stimulated EL4, and YAC-1 cell) were europium-labeled and a europium-release assay was performed as previously described.[32] Cytolytic activity was determined using the following formula: (% of lysis) = ((experimental europium-release − spontaneous europium-release)/(maximum europium-release − spontaneous europium-release)) × 100. Spontaneous europium-release of the target cells was < 15% of maximum europium-release by detergent.

Reverse transcription-polymerase chain reaction (RT-PCR) analysis of activation status of tumor-infiltrating immune cells
Tumors were collected 2 days after intratumoral injection in Protocol-1 and -2, and total RNA was isolated using Sepasol-RNA I Super (Nacalai Tesque, Inc., Kyoto, Japan), according to the manufacturer's instructions. RT proceeded for 60 min at 42°C in a 50 μl reaction mixture containing 5 μg total RNA treated with DNase I, 10 μl 5 × RT buffer, 5 mM $MgCl_2$, 1 mM dNTP mix, 1 μM

random primer (9-mer), 1 μM oligo(dT)$_{20}$, and 100 U ReverTra Ace (TOYOBO Co., Ltd, Osaka, Japan). PCR amplification of the perforin, granzyme B, IFN-γ, and β-actin transcripts was performed in 50 μl of a reaction mixture containing 1 μl of RT material, 5 μl 10 × PCR buffer, 1.25 U *Taq* DNA polymerase (TOYOBO Co., Ltd), 1.5 mM $MgCl_2$, 0.2 mM dNTP, and 0.4 μM primers. The sequences of the specific primers were as follows: murine perforin: forward, 5′-ttt cgc ctg gta caa aaa cc-3′; reverse, 5′-cag tcc tgg ttg gtg acc tt-3′; murine granzyme B: forward, 5′-ctc gac cct aca tgg cct ta-3′; reverse, 5′-gaa agg aag cac gtt tgg tc-3′; murine IFN-γ: forward, 5′-gct ttg cag ctc ttc ctc at-3′; reverse, 5′-tga gct cat tga atg ctt gg-3′; murine β-actin: forward, 5′-tgt gat ggt ggg aat ggg tca g-3′; reverse, 5′-ttt gat gtc acg cac gat ttc c-3′. After denaturation for 2 min at 95°C, 20 cycles of denaturation for 30 s at 95°C, annealing for 30 s at 60°C (for perforin and β-actin) or 62°C (for granzyme B and IFN-γ), and extension for 30 s at 72°C were repeated and followed by completion for 4 min at 72°C. The PCR product was electrophoresed through a 3% agarose gel, stained with ethidium bromide, and visualized under ultraviolet radiation. EZ Load (Bio-Rad Laboratories, Inc., Tokyo, Japan) was used as a 100 bp molecular ruler. The expected PCR product sizes were 680 bp (perforin), 507 bp (granzyme B), 379 bp (IFN-γ), and 514 bp (β-actin).

Results

Growth and histology of B16BL6 tumor injected with chemokine-expressing AdRGD

In order to evaluate the suppressive effect of *in vivo* chemokine-gene transduction against established tumor, we investigated the changes in tumor volume after intratumoral injection of each chemokine-expressing AdRGD in murine B16BL6 melanoma model (Figure 1). Growth of B16BL6 tumor injected with AdRGD-Luc (control vector) at 3×10^8 PFU was equal to that of vehicle-injected tumor. On the other hand, mice injected intratumorally with each chemokine-expressing AdRGD exhibited slight delay of tumor growth as compared with control groups, and the rank order of the suppressive effect in eight chemokine-treated groups was CCL19 = CCL21 = CCL27 > CCL17 = CCL20 = CCL22 = CX3CL1 > XCL1.

Next, histological changes of tumors injected with chemokine-expressing AdRGD were examined by HE staining (Figure 2a–d) and immunohistochemical staining against Ki-67 (a marker of proliferating cells; Figure 2e–h) and CD34 (a marker of vascular endothelial cells; Figure 2i–l). On day 2 after intratumoral injection, differences in frequency of granulocytic infiltration, size of necrotic area with undernourishment, proliferative state of tumor cells, and frequency of neovascularity were not observed among tumors injected with PBS, AdRGD-Luc, AdRGD-CCL17, and AdRGD-CCL19. Similar pathological findings were also observed in other tumors treated with AdRGD-CCL20, -CCL21, -CCL22, -CCL27, -XCL1, or -CX3CL1 (data not shown). These observations revealed that AdRGD particle itself or the expressed chemokines did not contribute directly to injury of tumor cells and did not facilitate formation/breakdown of tumor vessels. Therefore, the data suggested that a delay in growth of B16BL6 tumor in response to direct injection of chemokine-expressing AdRGD might be caused by promotion of immune cell infiltration into tumor tissue by the secreted chemokines.

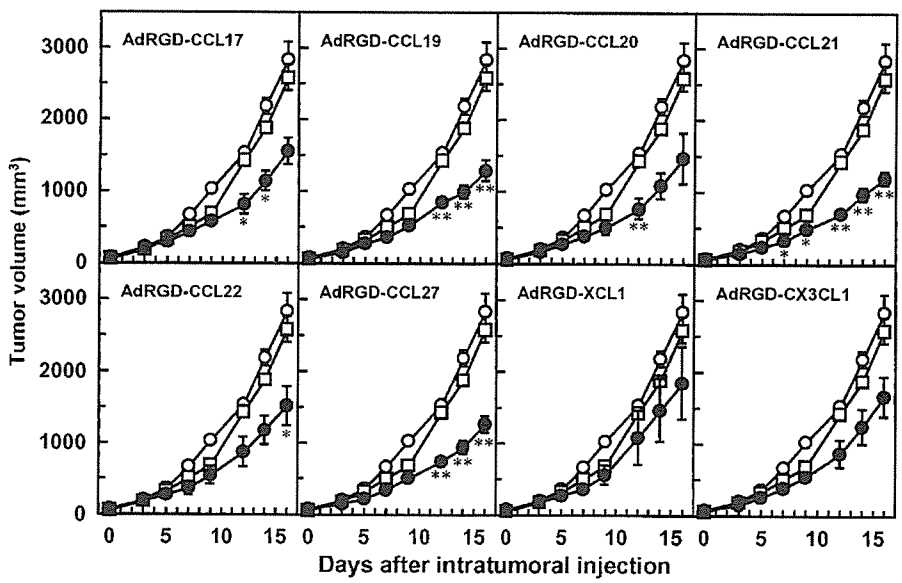

Figure 1 Anti-B16BL6 tumor efficacy of intratumorally injected chemokine-expressing AdRGD. B16BL6 cells were intradermally inoculated into the right flank of C57BL/6 mice at 4×10^5 cells/mouse. The tumors (5–7 mm in diameter) were injected with each chemokine-expressing AdRGD (●) or AdRGD-Luc (□) at 3×10^8 PFU. Likewise, PBS (○) was injected into the tumors. The tumor volume was calculated after measuring the major and minor axes of the tumor at indicated points. Each point represents the mean ± s.e. from 6 to 10 mice. Statistical analysis was carried out by Mann–Whitney *U*-test: $^*P<0.01$, $^{**}P<0.001$ versus AdRGD-Luc-injected group (□).

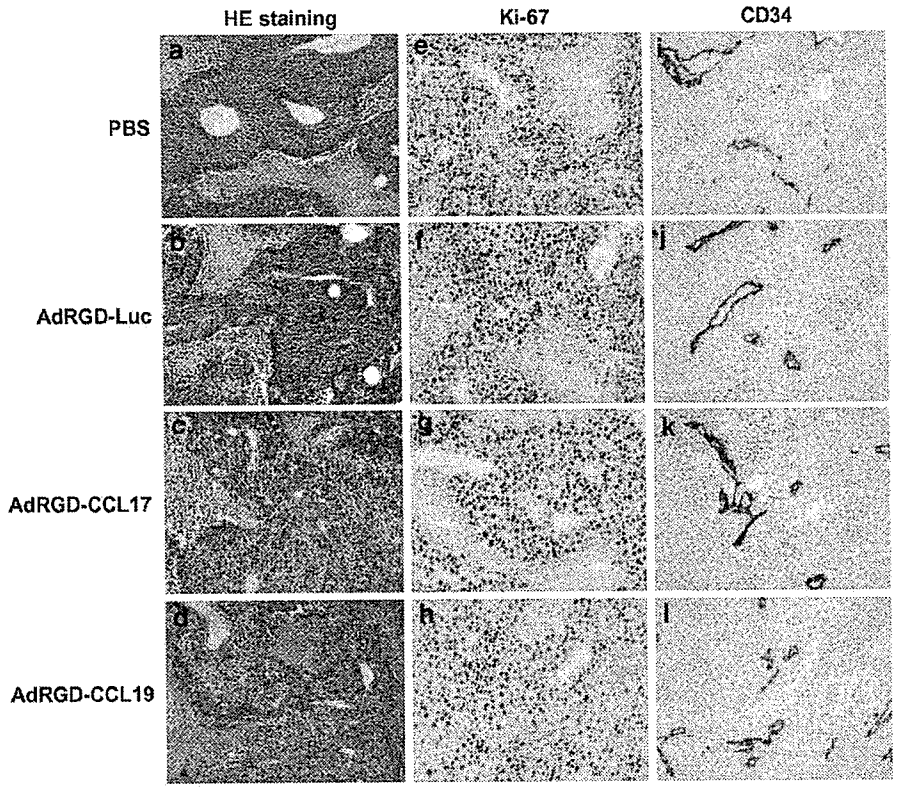

Figure 2 Histopathological and immunohistochemical examination of B16BL6 tumor injected with chemokine-expressing AdRGD. B16BL6 cells were intradermally inoculated into the right flank of C57BL/6 mice at 4×10^5 cells/mouse. The tumors (5–7 mm in diameter) were injected with AdRGD-Luc (**b**, **f**, **j**), AdRGD-CCL17 (**c**, **g**, **k**) or AdRGD-CCL19 (**d**, **h**, **l**) at 3×10^8 PFU. Likewise, PBS was administered into control tumors (**a**, **e**, **i**). On day 2 after intratumoral injection, HE staining (**a–d**) and immunohistochemical staining against Ki-67, to identify proliferating cells (**e–h**), and CD34, to identify vascular endothelial cells (**i–l**), were performed using paraffin-embedded tumor sections and frozen tumor sections, respectively. Original magnifications are ×200.

The subset and activation state of infiltrating immune cells in B16BL6 tumor injected with chemokine-expressing AdRGD

We attempted to identify the subset of infiltrating immune cells by immunohistochemical analysis in B16BL6 tumor 2 days after injection of chemokine-expressing AdRGD. In comparison with PBS-injected tumor, tumors injected with any AdRGD including control AdRGD-Luc exhibited increased F4/80-positive macrophage accumulation (Figure 3a–d), indicating that intratumoral administration of AdRGD induced inflammatory response in tumor tissue irrespective of the type of transgene. However, we determined that inflammation and macrophage-accumulation upon intratumoral injection of AdRGD would contribute little to the tumor suppressive effects induced by chemokine-expressing AdRGD because growth of B16BL6 tumor injected with AdRGD-Luc was comparable to that of PBS-injected tumor as shown in Figure 1. Notably, a large number of CD3-positive T cells were detected in tumors injected with AdRGD-CCL19, whereas T-cell accumulation in tumors injected with other chemokine-expressing AdRGD was moderately (AdRGD-CCL21), slightly (AdRGD-CCL17, -CCL20, -CCL22, and -CCL27), or not (AdRGD-XCL1 and -CX3CL1) different from that in control tumors (Figures 3e–h and 4a). In addition, subset analysis of the T cells that infiltrated the AdRGD-CCL19-injected tumor revealed that CCL19 induced significant infiltration of both $CD4^+$ and $CD8^+$ subsets, composed of helper T cells (Th) and CTLs, respectively, into tumor tissue (Figures 3m, n and 4a). However, most of these T cells attracted by CCL19 were not in a sensitized/activated state as demonstrated by the low amounts of perforin-positive cells in tumors injected with AdRGD-CCL19 (Figures 3o and 4a). Similarly, the perforin-positive cells were hardly recognized in tumors of several chemokine groups, which showed moderate increase of tumor-infiltrating $CD4^+$ and $CD8^+$ subsets (Figure 4a), indicating that intratumoral injection using our eight chemokine-expressing AdRGDs did not significantly attract activated effector cells that possessed potent killing activity against tumor cells. Considerable enhancement of NK cell-infiltration into parenchyma of tumor tissue was not observed in any groups injected with chemokine-expressing AdRGD (Figures 3i–l and 4a). On the other hand, intratumoral injection of AdRGD-CCL17 resulted in marked difference in the number of NK cells in the peritumoral portion as compared with the

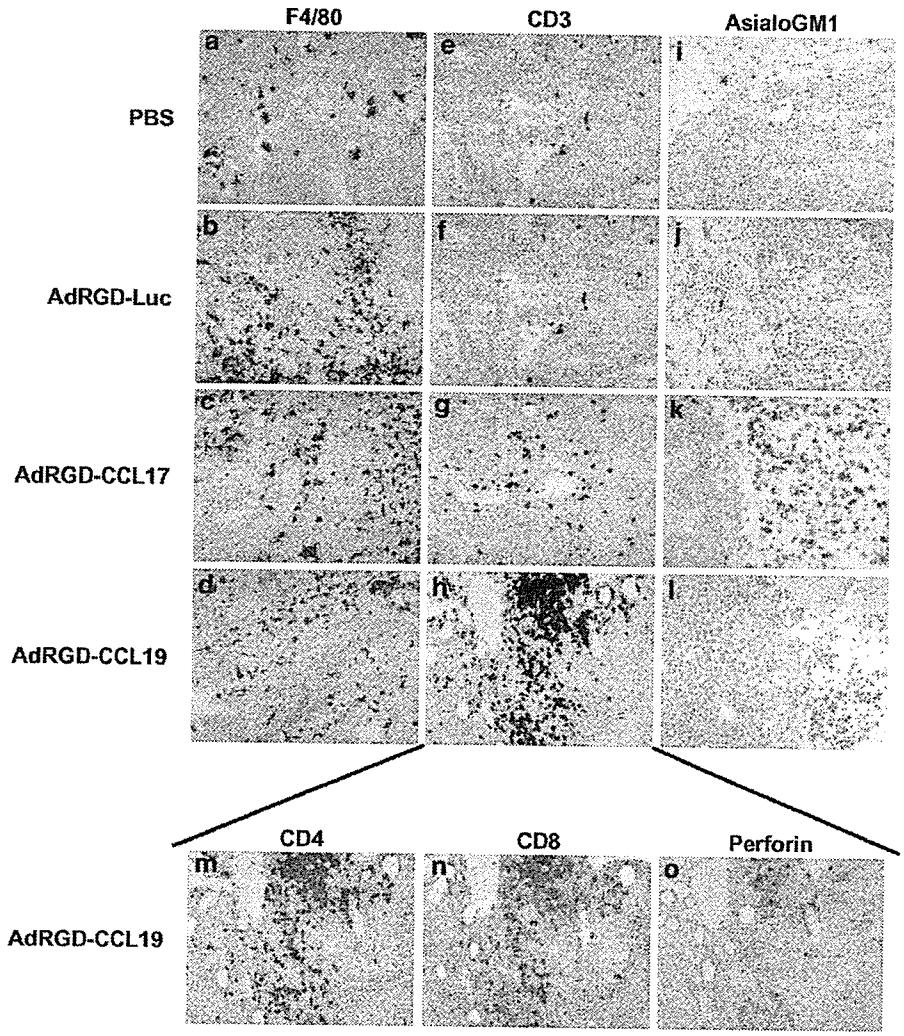

Figure 3 Infiltrating immune cell images in B16BL6 tumors injected with chemokine-expressing AdRGD. B16BL6 cells were intradermally inoculated into the right flank of C57BL/6 mice in at 4×10^5 cells/mouse. The tumors (5–7 mm in diameter) were injected with AdRGD-Luc (**b**, **f**, **j**), AdRGD-CCL17 (**c**, **g**, **k**), or AdRGD-CCL19 (**d**, **h**, **l**, **m**, **n**, **o**) at 3×10^8 PFU. Likewise, PBS was administered into control tumors (**a**, **e**, **i**). On day 2 after intratumoral injection, immunohistochemical staining against F4/80 (to detect macrophages; **a–d**), CD3 (for identification of T cells; **e–h**), and asialoGM1 (for identification of NK cells; **i–l**) was performed using frozen tumor sections. For determining the subset and the activation status of T cells in AdRGD-CCL19-injected tumor, immunohistochemical staining against CD4 (**m**), CD8 (**n**), and perforin (**o**) was performed using serial sections for h. Original magnifications are $\times 200$.

AdRGD-Luc-injected group, and moderate enhancement of NK cell-accumulation was observed at periphery of tumors injected with AdRGD-CCL19, -CCL21, or -CCL22 (Figures 3i–l and 4b). Immunostaining against CD11c showed that intratumoral injection of each chemokine-expressing AdRGD could not induce significant accumulation of DCs, which are the most potent antigen-presenting cells (Figure 4a).

Taken together, these data demonstrate that intratumoral injection of AdRGD-CCL19 drastically promotes T-cell infiltration into B16BL6 tumor tissue, and AdRGD-CCL17 injection most efficiently induces NK cell-accumulation at the peritumoral area, but not inside the tumor tissue. Moreover, perforin-positive immune cells were detected at extremely low levels in all tumors, suggesting that the tumor-infiltrating naive T cells attracted by chemokine gene transduction should be activated in tumor-specific manner in order to achieve more effective tumor elimination.

Anti-B16BL6 tumor efficacy of combinational therapy using gp100/DC-immunization and intratumoral injection of chemokine-expressing AdRGD

We theorized that combination therapy, which includes a treatment that can activate tumor-specific immune response in the host, might be required for more effective application of chemokine-expressing AdRGD to cancer immunotherapy. We previously demonstrated that vaccination with DCs transduced with gp100, a melanoma-associated antigen, by using AdRGD could induce potent protective effects against murine B16BL6 melanoma challenge based on enhancement of gp100-specific CTL

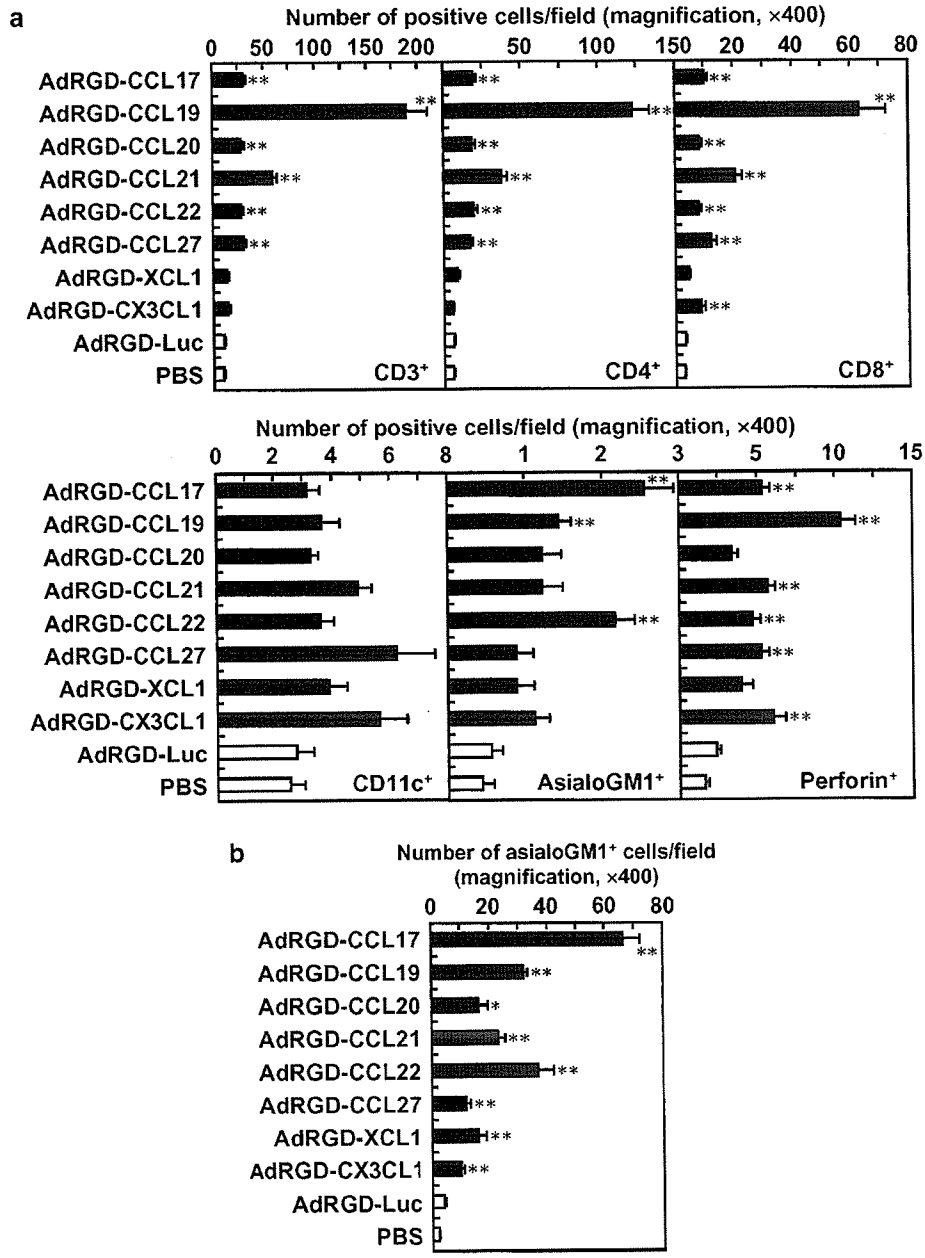

Figure 4 Identification of tumor-infiltrating immune cells in B16BL6 tumors injected with chemokine-expressing AdRGD. B16BL6 cells were intradermally inoculated into the right flank of C57BL/6 mice at 4×10^5 cells/mouse. The tumors (5–7 mm in diameter) were injected with each chemokine-expressing AdRGD or AdRGD-Luc at 3×10^8 PFU. Likewise, PBS was administered into control tumors. On day 2 after intratumoral injection, immunohistochemical staining against CD3, CD4, CD8, asialoGM1, perforin, and CD11c was performed using frozen tumor sections. Then, the number of positive cells in intratumoral (**a**) or peritumoral (**b**) sections was assessed by counting six fields per specimen under × 400-magnification . The data represent the mean ± s.e. of results from three tumors. Statistical analysis was carried out by Welch's *t*-test: $^*P<0.01$, $^{**}P<0.001$ versus AdRGD-Luc-injected group.

activity.[33] Thus, antitumor efficacy of a treatment combining intradermal immunization of gp100/DCs and intratumoral injection of chemokine-expressing AdRGD was investigated in B16BL6 tumor-bearing mice, according to the Protocol-2 described in the Materials and methods section.

In order to confirm the activation of systemic immunity in tumor-bearing mice immunized with gp100/DCs, we first evaluated CTL activity in splenocytes from these mice. Single immunization with gp100/DCs at a site distant from the tumor-inoculation site could promote killing activity of effector cells targeting B16BL6 cells (Figure 5a). As H-2 haplotype-matched irrelevant EL4 cells and YAC-1 cells, which are highly susceptible to NK activities, were not injured by these effector cells (Figure 5b and c), gp100/DC-administration could sensitize and activate gp100-specific CTLs in B16BL6 tumor-bearing mice as well as intact mice. As shown in Figure 6, mice

injected intratumorally with PBS after gp100/DC-immunization did not exhibit considerable suppression of B16BL6 tumor growth as compared with unimmunized group, indicating that regression of B16BL6 tumor that had begun to proliferate was very difficult with only a single dose of gp100/DCs. At initial stage until day 11 after intratumoral injection, tumor growth in mice treated with AdRGD-Luc after gp100/DC-immunization was obviously delayed as compared with that in the PBS-injected group. We speculated that this suppressive effect was based on the activity of immune cells, including activated CTLs, which were attracted to tumor tissue by an inflammatory response to AdRGD-administration. In comparison with the control groups, AdRGD-CCL19 injection, which induced massive tumor-infiltrating T cells in unimmunized mice, only slightly delayed tumor growth in gp100/DC-immunized mice, although the effect was better than that by injection of AdRGD-CCL20 or -CCL21. Intratumoral injection of AdRGD-XCL1 or -CX3CL1 was not effective for promoting the tumor suppressive effect based on gp100/DC-immunization. On the other hand, intratumoral injection of AdRGD-CCL17, -CCL22, or -CCL27 in combination with gp100/DC-immunization could remarkably improve anti-tumor efficacy.

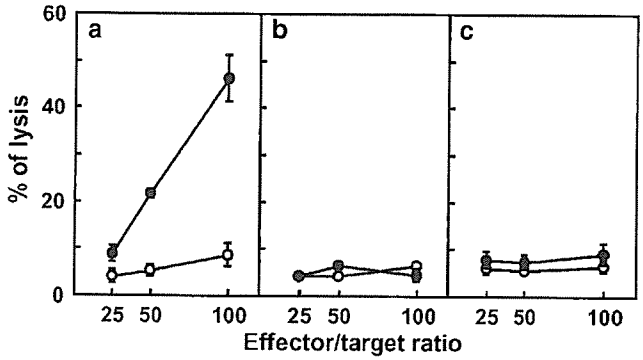

Figure 5 Enhanced tumor-specific CTL activity in B16BL6 tumor-bearing mice by gp100/DC-immunization. B16BL6 cells were intradermally inoculated into the right flank of C57BL/6 mice at 4×10^5 cells/mouse. One day later, the mice were intradermally injected with 10^6 gp100/DCs (●) or PBS (○) in the left flank. At 1 week after immunization, nonadherent splenocytes were prepared from these mice, and then were restimulated *in vitro* for 5 days with IFN-γ-stimulated and mitomycin C-inactivated B16BL6 cells. A cytolytic assay using the restimulated splenocytes was performed against IFN-γ-stimulated B16BL6 (**a**), IFN-γ-stimulated EL4 (**b**), and YAC-1 (**c**) cells. The data represent the mean±s.e. of three independent cultures from three individual mice.

Accumulation and activation state of immune cells in tumor treated with the combination of gp100/DC-immunization and chemokine-expressing AdRGD injection

B16BL6 tumors were harvested 2 days after intratumoral injection of chemokine-expressing AdRGD (Protocol-2) and were analyzed for the levels of infiltrating T cells by immunohistochemical staining. As shown in Figure 7, tumors injected with AdRGD-CCL17, -CCL22, or -CCL27 exhibited enhanced $CD3^+$ T-cell accumulation,

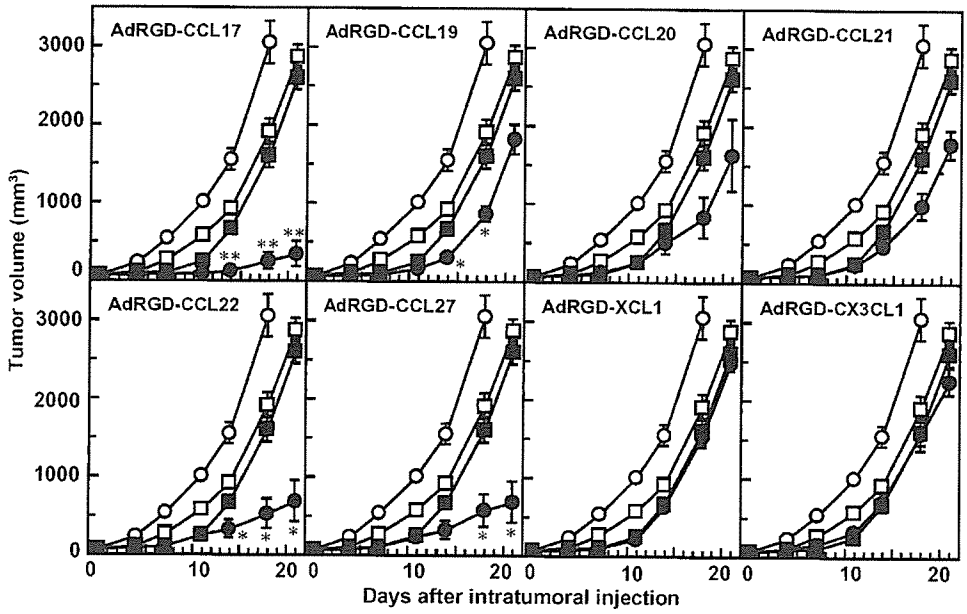

Figure 6 Anti-B16BL6 tumor efficacy of intratumorally injected chemokine-expressing AdRGD in combination with gp100/DC immunization. B16BL6 cells were intradermally inoculated into the right flank of C57BL/6 mice at 4×10^5 cells/mouse. The next day post-tumor inoculation, the mice were intradermally immunized with 10^6 gp100/DCs (●, ■, □) or PBS (○) in the left flank. Then, the tumors (5–7 mm in diameter) were injected with each chemokine-expressing AdRGD (●) or AdRGD-Luc (■) at 3×10^8 PFU. Likewise, PBS was administered into control tumors in mice pretreated with gp100/DCs (□) or PBS (○). Tumor volume was calculated after measuring the major and minor axes of the tumor at indicated points. Each point represents the mean±s.e. of 7–15 mice. Statistical analysis was carried out by Mann–Whitney *U*-test: $^*P<0.01$, $^{**}P<0.001$ versus AdRGD-Luc-injected group (■).

whereas the number of T cells in tumor tissue was only slightly elevated by injection of AdRGD-CCL19, -CCL20, or -CCL21, and did not change between the AdRGD-XCL1- or AdRGD-CX3CL1-injected group and the AdRGD-Luc-injected group. These data disagreed with the observation that intratumoral injection of AdRGD-CCL19 could attract a large number of T cells in mice without gp100/DC-immunization as shown in Figures 3h and 4a, suggesting that responsiveness of T cells for chemokines was altered by the activation state of the host's immune system, that is, sensitization of T cells by gp100/DC-administration. Importantly, the levels of tumor-infiltrating T cells showed positive correlation for antitumor efficacy (Figure 6) in mice treated with gp100/DC immunization and each chemokine-expressing AdRGD injection. Because the number of infiltrating NK cells and DCs was low in tumors injected with any AdRGD in this combinational protocol as well as in Protocol-1 (data not shown), we theorized that infiltrating CTLs were the major effector cells responsible for improved anti-B16BL6 tumor effects.

In order to evaluate the activation state of tumor-associated CTLs, we performed RT-PCR analysis specific for perforin, granzyme B, and IFN-γ, which are the major cytotoxic molecules and secreted cytokines in activated CTLs (Figure 8). We focused on tumors treated with AdRGD-CCL17 and AdRGD-CCL19, which induced the most effective T-cell infiltration in Protocol-2 and -1, respectively. The combination with gp100/DC-immunization notwithstanding, PCR products derived from transcripts of perforin, granzyme B, or IFN-γ were detected at higher levels in tumors injected with AdRGD-CCL17 or AdRGD-CCL19 as compared with AdRGD-Luc-injected tumors. In the absence of gp100/DC immunization, AdRGD-CCL19-injected tumors expressed more perforin- and granzyme B-specific mRNA than AdRGD-CCL17-injected tumors, whereas intratumoral injection of AdRGD-CCL17 in combination with gp100/DC immunization induced higher perforin, granzyme B, and IFN-γ mRNA expression in tumor tissue than AdRGD-CCL19 injection. In addition, expression levels of perforin, granzyme B, and IFN-γ mRNA were increased in AdRGD-CCL17-injected groups by receiving gp100/DC immunization. On the other hand, gp100/DC immunization of AdRGD-CCL19-injected groups tended to decrease or did not alter mRNA expression levels of these three activation markers. Though intratumoral injection with AdRGD-CCL19 in protocol-1 was able to induce T-cell infiltration much more efficiently than AdRGD-CCL17 injection in protocol-2 (Figures 4a and 7c), RT-PCR analysis revealed that AdRGD-CCL17-injected tumor in gp100/DC-immunized mice contained

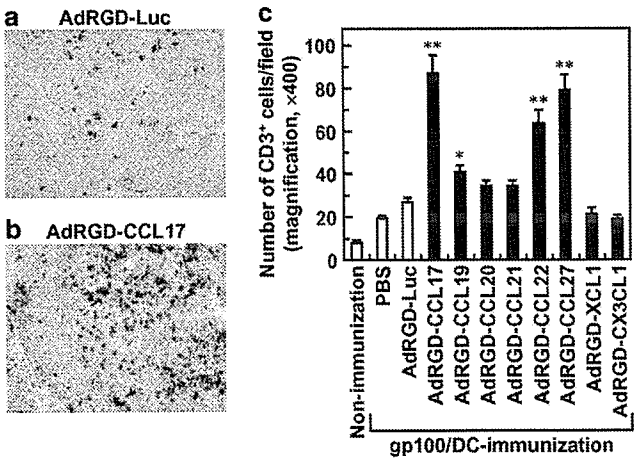

Figure 7 Infiltration of T cells into B16BL6 tumors of mice treated with the combination of gp100/DC-immunization and intratumoral injection of chemokine-expressing AdRGD. B16BL6 cells were intradermally inoculated into the right flank of C57BL/6 mice at 4×10^5 cells/mouse. The next day, the mice were intradermally injected with 10^6 gp100/DCs in the left flank. Then, the tumors (5–7 mm in diameter) were injected with each chemokine-expressing AdRGD or AdRGD-Luc at 3×10^8 PFU. Likewise, PBS was administered into control tumors. On day 2 after intratumoral injection, immunohistochemical staining against CD3 for determining T cells was performed with frozen tumor sections. (**a** and **b**) Original magnifications are ×200. (**c**) The number of CD3-positive cells in the intratumoral section was assessed by counting six fields per specimen under ×400-magnification. The data represent the mean±s.e. of results from three tumors. Statistical analysis was carried out by Welch's *t*-test: $^*P<0.01$, $^{**}P<0.001$ versus AdRGD-Luc-injected group.

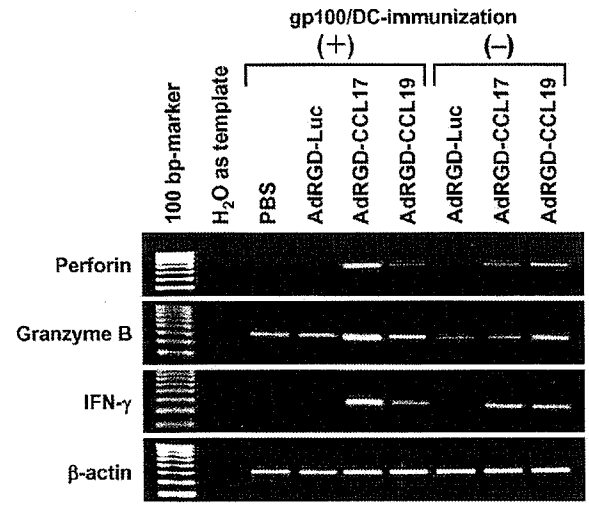

Figure 8 Activation state of infiltrating immune cells in B16BL6 tumors injected intratumorally with chemokine-expressing AdRGD in combination with or without gp100/DC-immunization. B16BL6 cells were intradermally inoculated into the right flank of C57BL/6 mice at 4×10^5 cells/mouse. After 1 day, the mice were intradermally injected with (Protocol-2) or without (Protocol-1) 10^6 gp100/DCs in the left flank. The tumor (5–7 mm in diameter) in Protocol-1 or -2 was injected with AdRGD-CCL17, AdRGD-CCL19, or AdRGD-Luc at 3×10^8 PFU. Likewise, PBS was administered into control tumors. After 2 days, total RNA was isolated from the tumors collected from these mice, and then RT-PCR, specific for perforin, granzyme B, and IFN-γ transcripts, was performed as described in the Materials and methods section. The PCR products were electrophoresed through a 3% agarose gel, stained with ethidium bromide, and visualized under ultraviolet light.